Full paper

The influence of FEC on the solvation structure and reduction reaction of LiPF$_6$/EC electrolytes and its implication for solid electrolyte interphase formation

Tingzheng Hou[a,b], Guang Yang[c], Nav Nidhi Rajput[b,d], Julian Self[a,b], Sang-Won Park[a,b], Jagjit Nanda[c], Kristin A. Persson[a,b,*]

[a] Department of Materials Science and Engineering, University of California Berkeley, 210 Hearst Mining Building, Berkeley, CA, 94720, United States
[b] Energy Technologies Area, Lawrence Berkeley National Laboratory, Berkeley, CA 94720, United States
[c] Chemical Sciences Division, Oak Ridge National Laboratory, Oak Ridge, TN, 37831, United States
[d] Department of Chemical and Biological Engineering, Tufts University, Medford, MA, 02155, United States

ABSTRACT

Fluoroethylene carbonate (FEC) has been proposed as an effective electrolyte additive that enhances the stability and elasticity of the solid electrolyte interphase (SEI) of emerging Si and Li metal anodes. However, uncertainties still remain on the exact mechanism through which FEC alters the electrolyte decomposition and SEI formation process. Herein, the influence of FEC on LiPF$_6$/ethylene carbonate (EC) electrolytes for Si anodes is investigated through classical molecular dynamics, Fourier-transform infrared spectroscopy, and quantum chemical calculations. Albeit a minority species, FEC is found to significantly modify the solvation structure and reduction behavior of the electrolyte while being innocuous to transport properties. Even with limited 10% of FEC, the Li$^+$ solvation structure exhibits a notably higher contact-ion pair ratio (14%) than the parent EC electrolyte (6%). Moreover, FEC itself, as a new fluorine-containing species, appears in 1/5 of the Li$^+$ solvation shells. The Li$^+$-coordinated FEC is found to reduce prior to EC and uncoordinated FEC which will passivate the anode surface at an early onset (ca. 0.3 V higher than EC) by forming LiF. The critical role of FEC in tailoring the Li$^+$ solvation structure and as-formed protective SEI composition provides mechanistic insight that will aid in the rational design of novel electrolytes.

1. Introduction

To realize next-generation energy storage systems, there is a pressing need for functional, optimized electrolytes with excellent bulk stability and conductivity while exhibiting a suitable range of passivating reactions towards the chosen anode material [1,2]. Mounting evidence points to rational design of the bulk electrolyte solvation structure [3], including both majority as well as minority species, as a vehicle towards tailoring specific interfacial reactivity and reduction potentials of electrolyte components, which in turn contribute to the formation of a functional solid electrolyte interphase (SEI) layer.

An optimal SEI layer passivates the anode surface against further side reactions while facilitating Li-ion transport [4,5]. Extensive previous work shows that a complicated cascade of reduction reactions occurs during the first cycle, and that the initially formed SEI

containing inorganic species, e.g. LiF and Li$_2$CO$_3$ [6,7], as well as organic ones, e.g. lithium ethylene dicarbonates (LEDC) [8,9], further evolves through a variety of aging processes [10–13] (hydrolysis, reaction between Li salt and intermediate decomposition products, and thermal decomposition, etc.) as well as continuous electrolyte reduction [14,15]. The sequence of reactions and their aging depend both on the specific components and concentration, including additives and impurities, of the bulk electrolyte, and upon the specific anode material and its surface chemistry and structure. Hence, in principle, every anode material requires a differently tailored electrolyte, to achieve maximal compatibility—both electrochemically as well as mechanically.

One of the most promising anode materials for future high energy density Li-ion batteries (LIBs) is Si, due to its high theoretical specific capacity (exceeding 4200 mAh g^{-1}) and low cost [16]. However,

conventional LIB electrolytes, such as lithium hexafluorophosphate (LiPF$_6$) in cyclic ethylene carbonate (EC) and linear dimethyl carbonate (DMC) and/or diethyl carbonate (DEC) [17,18,119], form a non-passivating Si SEI that is unable to mitigate the cracking due to Si's large volume expansion and contraction during cycling. To improve the Si SEI performance, several approaches [19] have been explored, e.g., nanostructuring [20,21], use of binders with tailored functionalities [22–24], as well as modified salts and electrolyte additives [25,26], fluoroethylene carbonate (FEC) has recently been proposed as an effective electrolyte additive that significantly enhances the stability and elasticity of the as-formed SEI film [27,28]. In the presence of FEC, which degrades at a higher reduction potential than both EC and DEC, a denser, more uniform and conformal SEI is formed on the silicon electrode [19]. This SEI layer has been found to ameliorate the emergence of large cracks and suppress further decomposition of EC/DMC, leading to enhanced electrochemical performance and improved coulombic efficiency [19]. To understand the composition and morphology of the Si SEI formed with FEC, extensive experiments using scanning transmission electron microscopy (STEM) [29], electron energy loss spectroscopy (EELS) [29], Fourier-transform infrared spectroscopy (FTIR) [25,30], X-ray photoelectron spectroscopy (XPS) [16,31], atomic force microscopy (AFM) [32,33], hard X-ray photoelectron spectroscopy (HAXPES) [19,34], nuclear magnetic resonance (NMR) [16,35], differential electrochemical mass spectrometry (DEMS) [36], and time-of-flight secondary ion mass spectrometry (ToF-SIMS) [37], etc., have been undertaken. Lucht [25] and co-workers recommended a 10% FEC inclusion based on a combination of low impedance and high capacity retention due to the formation of an SEI which contains both a flexible polymer and high lithium salt content (LiF and Li$_2$CO$_3$). Subsequent studies found that, compared with a standard EC/DMC electrolyte, the use of 10% FEC additive modifies the organic SEI components derived from LEDC and soluble linear oligomers to soluble and insoluble crosslinked poly(ethylene oxide)-based polymers (such as lithium poly(vinylene carbonate)), which could better passivate the anode surface and resist volume expansion [16,35,38]. Meanwhile, FEC incurs increased formation of LiF, less formation of Li$_2$CO$_3$ and organic carbonate species resulting in an overall lower interfacial impedance of the Si anode [39]. The presence of fluoride species further leads to the etching of the native oxide surface layer, improving the surface region Li conductivity and lowering the interfacial resistance [4,29]. Moreover, there is evidence that FEC influences the LiPF$_6$ decomposition reaction and may suppress further salt degradation after the initial cycles [19].

Numerous studies have endeavored to understand the reaction pathway and SEI formation mechanism through experiments [40] and multiscale computational simulations [41]. For example, experimental efforts have utilized Lithium Naphthalide (LiNap) as a one-electron reduction reagent [42,43] to analyze the resulting solid precipitates and gas evolution. Through this technique, FEC was found to decompose into a range of products including HCO$_2$Li, Li$_2$C$_2$O$_4$, Li$_2$CO$_3$, and polymerized vinylene carbonate (VC), which supports a decomposition mechanism where FEC reduces to form VC and LiF, followed by subsequent VC reduction. Other complementary approaches include theoretical modeling the electrolyte [44], Si anode [45], and their interphase [46,47]. Quantum chemical calculations confirm that defluorination reactions significantly increase the reduction potential of FEC [48]. Leung and Balbuena et al. have pioneered the *ab-initio* molecular dynamics (AIMD) simulation of EC and FEC on the surface of Si as well as lithiated Si (LiSi$_4$, LiSi$_2$, LiSi and Li$_{13}$Si$_4$) [49–52] including the native oxide layer [45,53], and proposed a series of possible decomposition mechanisms leading to LiF formation and polymerization. FEC is found to exhibit more diverse reaction pathways than the two-electron reduction of unsubstituted ethylene carbonate [54–56]. Both one- and two-electron reactions are feasible for the FEC reduction and result in a fluoride radical which in both cases contribute to the formation of LiF [52]. Also, it was found that radical species are

responsible for the electron transfer that allows SEI layer growth once its thickness has evolved beyond the electron tunneling regime [46,57,58]. While several studies have focused on the reduction mechanisms of single FEC [59] and simplified solvation/interface models [52,60], a thorough examination of the influence of FEC on the solvation structure of the electrolyte [61], and hence the reduction potentials of the associated majority as well as minority species whose populations are altered by FEC, has to our knowledge not been undertaken. For example, it has been widely assumed that FEC, exhibiting a lower donor number than EC, remains largely uncoordinated as an additive in LIB electrolyte formulations [62,63]. However, even as a minority species, FEC may strongly influence the reduction potential and decomposition mechanism of associated electrolyte components, and hence alter the onset as well as reaction sequence of the bulk electrolyte. One of the goals of this contribution is to investigate how FEC influences the solvation structure, which further determines the reduction reactions and the subsequent SEI formation process.

In the present work, we report classical molecular dynamics (MD) simulations coupled with first-principles quantum mechanics to describe the detailed solvation structure and reactivity of LiPF$_6$ in EC/FEC, as a function of FEC as well as salt concentration. The solvation structure, self-diffusion coefficient and other macroscopic properties of the EC/LiPF$_6$ electrolyte with or without FEC additive are obtained, and the reduction potentials of the majority as well as minority species are calculated. Spin density analysis was used to further elucidate the reduction behavior of the solvate complexes obtained from the MD simulation, and hence the role of FEC in the SEI formation reaction. Corresponding experimental FTIR measurements are used for validation and as a direct determination of the coordination number in comparison with the calculated solvation structure. The aim of our work is to provide a deeper understanding of the subtle influence of the FEC additive on the bulk electrolyte and its constituents to aid in future rational design of functional electrolytes for Si anodes.

2. Calculation methods

2.1. Classical molecular dynamics (MD)

MD simulations were performed using the Large Scale Atomic/Molecular Massively Parallel Simulator (LAMMPS) [64] code for electrolytes of 1.0/1.2 M LiPF$_6$ in EC or EC with 5/10 mol% FEC. Although cyclic solvents are often used together with linear solvent ingredients such as DEC or DMC to modify viscosity, it was found that when EC contributes more than 50% by weight of the electrolyte, EC becomes, to good approximation, the exclusive "inner member" of the Li$^+$ solvation sheath [65]. Hence, only EC (and FEC) molecules are considered here to simplify the model. 1500 solvent molecules were used as bulk electrolytes. The number of salt molecules was adjusted via several test runs for 1 atm and 298 K equilibrium conditions to achieve the 1.0 M and 1.2 M concentrations. Specifically, the final number of salt molecules were 104 and 126 with equilibrated box volume of 177.5 nm^3 and 180.2 nm^3, respectively. The molecules were initially packed randomly in a cubic box of size 54 × 54 × 54 Å^3 periodic in the XYZ direction using PACKMOL [66] (Figure S1, available in the supplementary material). The initial configuration was minimized by conjugated-gradient energy minimization scheme employing a convergence criterion of 1.0×10^{-4}. While the thermodynamic melting point for EC with 1 M LiPF$_6$ is approximately 298 K [67], the kinetic liquid range limit may be lower [68], which allows a room temperature liquid state simulation. The systems were equilibrated for 2 ns in the isothermal-isobaric ensemble (constant NPT) using the Parrinello–Rahman barostat to maintain a pressure of 1 bar and a temperature of 298 K with a time constant of 1 ps. An annealing process was conducted to further guarantee that all systems are melted and to avoid local configuration confinement. All systems were heated from 298 K to 400 K for 1 ns, and maintained at 400 K for 1 ns, and subsequently annealed from 400 to 298 K in 1 ns.

Finally, the production runs of 5 ns were conducted in the canonical ensemble (NVT) under Nose-Hoover thermostats with a time constant of 1 ps at 298 K. The simulation time was long enough to sample adequately the Fickian (diffusive) regime of all systems, which was justified by a 55 ns long run (Figure S2).

A non-polarizable force field model was employed, which is defined by the following potential functions:

$$E_{total}(r^N) = E_{bonds} + E_{angles} + E_{dihedrals}(+E_{impropers}) + E_{nonbonded} \tag{1}$$

$$E_{bonds} = \sum_{bonds} K_r (r - r_0)^2 \tag{2}$$

$$E_{angles} = \sum_{angles} K_\theta (\theta - \theta_0)^2 \tag{3}$$

$$E_{dihedrals} = \sum_{dihedrals} V [1 + cos(n\phi - d)] \tag{4}$$

$$E_{impropers} = \sum_{impropers} V [1 + dcos(n\phi)] \tag{5}$$

$$E_{nonbonded} = \sum_{i>j} 4\varepsilon_{ij} \left[\left(\frac{\sigma_{ij}}{r_{ij}} \right)^{12} - \left(\frac{\sigma_{ij}}{r_{ij}} \right)^6 \right] + \sum_{i>j} \frac{Cq_i q_j}{\varepsilon r_{ij}}, \ r < r_c,$$

$$\varepsilon_{ij} = \sqrt{\varepsilon_{ii}\varepsilon_{jj}}, \ \sigma_{ij} = \frac{\sigma_{ii} + \sigma_{jj}}{2} \tag{6}$$

The bonded interactions (bonds, angles, dihedrals, and impropers) were modeled as harmonic functions and the nonbonded included van der Waals interactions and Coulombic forces. The bonded and non-bonded parameters for EC and FEC were obtained from the Optimized Potentials for Liquid Simulations All Atom (OPLS-AA) force fields [69,70], the PF_6^- anion from Lopes et al. [71], and the lithium cations from Jensen et al. [72] The partial atomic charges for all molecules were derived by first optimizing the geometry using Becke's three-parameter exchange function combined with the Lee–Yang–Parr correlation functional (B3LYP) [73] at the aug-cc-pvdz theory level using the Gaussian 16 [74] package and then fitting the electrostatic potential surface using the RESP method [75,76]. Long-range electrostatic interactions were handled by the particle-particle particle-mesh (PPPM) solver with a grid spacing of 0.1 nm. A cutoff distance of 1.5 nm was used for electrostatic and 12–6 Lennard-Jones interactions. Moreover, each Li ion in the system is surrounded by at least one PF_6^- in the first solvation shell or second solvation shell according to the trajectories (Figure S3). Hence, if we ignore the negligible amount of aggregates (AGG), all Li ions can be categorized into the contact ion pair (CIP) and solvation separated ion pair (SSIP). A Boltzmann factor was used to estimate the CIP formation free energy from the population difference of the CIP and SSIP structures.

$$\Delta_f G_{CIP} = -k_B T \ln \frac{p(CIP)}{p(SSIP)} \tag{7}$$

where p is the population for each species, $\Delta_f G_{CIP}$ is their relative free energy, k_B is the Boltzmann constant and T is the temperature. For NVT run under equilibrated pressure, the Helmholtz free energy (A) is approximately equal to the Gibbs free energy (G).

To further examine the influence of FEC on the bulk electrolyte, transport properties are characterized by the self-diffusion constant (D) and the transference number (t_{Li}^+). The self-diffusion coefficients for Li^+, PF_6^-, EC, and FEC were extracted from the MD simulation by analysis of the mean square displacement (MSD) over time using the Stokes−Einstein relation [77]. The slope of the linear regime in the MSD was obtained for each simulation duration of 1 ns and averaged over 5 ns of the production runs to obtain:

$$D = \frac{1}{6} \frac{\langle (\delta r)^2 \rangle}{\Delta t} \tag{8}$$

Based on the self-diffusion constants, the Li^+ ionic transference number t_{Li}^+, was calculated from ratios of D according to Ref. [78]:

$$t_{Li^+} = \frac{D_{Li^+}}{D_{Li^+} + D_{PF_6^-}} \tag{9}$$

2.2. Quantum chemical calculations

Geometries of solvate complex were optimized from the initial structures observed in MD simulations to obtain their theoretical IR vibrations using Gaussian 16 at the B3LYP/6–31++G(d) level of theory [79]. The calculated IR data was then accumulated according to the composition ratio from the MD simulations to obtain the total spectra of each electrolyte. The adiabatic reduction potentials for the representative solvation structures were calculated using the following function [80].

$$E_{adiabatic} = -(G_{reduced} - G_{inital} + \Delta G_{solv}^o (reduced) - \Delta G_{solv}^o (initial)) / F - 1.4V \tag{10}$$

where $G_{reduced}$ and G_{inital} are the free energies of the reduced and initial complexes at 298.15 K in gas-phase at 298.15 K, respectively; ΔG_{solv}^o are the corresponding free energies of solvation, and F is the Faraday constant. The zero-point energy (ZPE) corrections were considered in the calculation while the basis set superposition error (BSSE) energy was neglected [81]. The solvent effects in the free energy calculation of each complex were considered using both an explicit cluster model and an implicit polarizable continuum model (PCM) [82]. The inclusion of empirical dispersion correction [83] resulted in very slight changes in reduction potentials $\leq$ 0.05 V (Table S1), and therefore was not included. A standard-state correction [84] was also considered to account for the four reduction reactions with free EC or PF_6^- generation, which resulted in the addition of a correction constant (RTln(24.47/M), where R is the gas constant, T is temperature, 24.47 is the molar volume in liter for ideal gas under 1 atm and 298.15 K, M = 1 for PF_6^-, M = 0.07 for EC) to ΔG_{solv}^o. A dielectric constant of 90 was adopted for the EC solvent as well as the EC/FEC mixture [85]. Geometries were allowed to relax after the electron transfer. Subtraction of 1.4 V accounts for the conversion from the absolute electrochemical scale to the commonly used Li/Li$^+$ potential scale in order to compare predicted values with experimental data using the same reference electrode. An additional factor of ca. 0.1 V for graphite intercalation or 0.3–0.4 V for Si anode Li insertion should be subtracted if the reference electrode is changed to these specific systems. The spin density calculation of the reduced state structures was conducted using natural bond orbital (NBO) theory. The dipole moment calculation was conducted at the B3LYP/6–311++G(d,p) level of theory.

3. Experimental methods

3.1. Fourier-transform infrared spectroscopy (FTIR)

The FTIR spectra for 1.0 M LiPF$_6$ in EC and 1.0 M LiPF$_6$ in EC with 10 wt% FEC were collected with a FTIR spectrometer (Bruker, ALPHA) using a diamond attenuated total reflection (ATR) accessory. Two pure solutions (EC and EC w/10 wt% FEC) were also tested as a comparison. Spectra were collected in the region from 4000 to 650 cm^{-1} with 128 scans and 2 cm^{-1} resolution in an argon-filled glovebox with O$_2$ and H$_2$O < 0.1 ppm. Ethylene carbonate (EC, anhydrous, $\geq$ 99%), lithium hexafluorophosphate (LiPF$_6$, battery grade) and fluoroethylene carbonate (FEC, 99%) were purchased from BASF. All spectra were normalized via stretching band of –CH$_2$ at 3000 cm^{-1}. This analysis is based upon the assumption that the infrared intensities of the uncoordinated and coordinated structures are equivalent after normalization (no scaling of the bands).
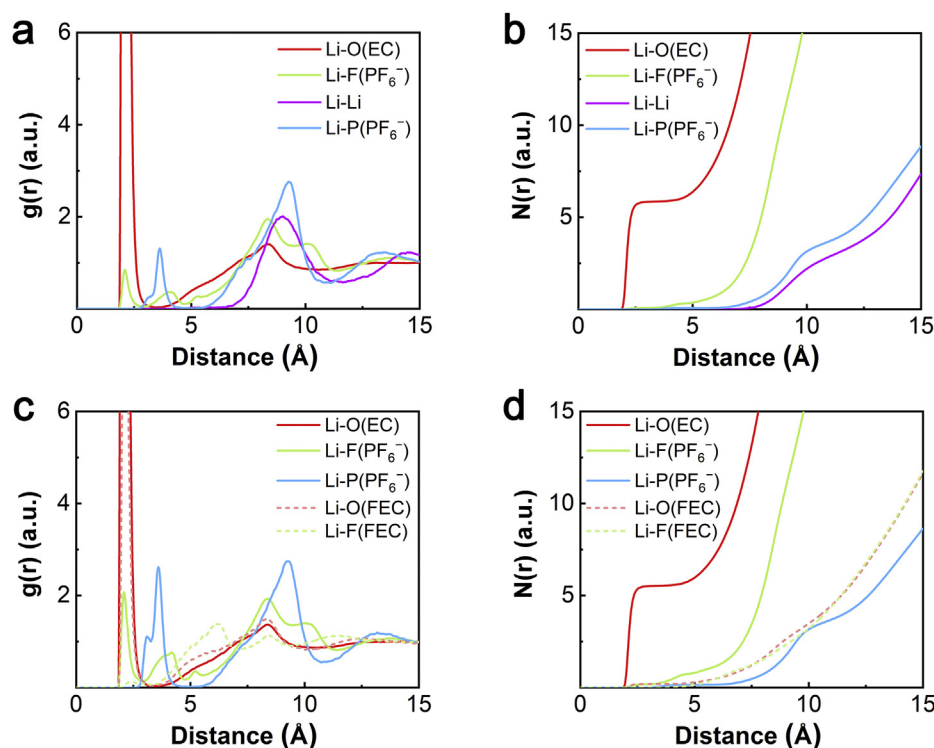
Fig. 1. Calculated radial distribution functions, $g(r)$, and the corresponding integrals, $N(r)$, of Li–O(EC), Li–F(PF$_6^-$), Li–Li, Li–P(PF$_6^-$) pairs of (a) (b) 1.0 M LiPF$_6$ in EC, and Li–O(EC), Li–F(PF$_6^-$), Li–P(PF$_6^-$), Li–O(FEC), Li–F(FEC) pairs of (c) (d) 1.0 M LiPF$_6$ in EC with 10%mol FEC additive.

4. Results and discussion

4.1. Solvation structure

A sequential simulation for 1.0/1.2 M LiPF$_6$ in EC with 0/5/10% FEC was conducted to investigate the influence of FEC on the solvation structure of the LiPF$_6$/EC electrolyte. The population proportion of solvent molecule and anion in the first solvation shell of Li$^+$ is clearly altered after adding FEC, which is confirmed by the radial distribution function, $g(r)$, and the corresponding integrals, $N(r)$, of Li-X (X = O (EC), F(PF$_6^-$), Li, P(PF$_6^-$) for EC and X = O(EC), F(PF$_6^-$), O(FEC), P (PF$_6^-$), F(FEC) for EC w/FEC) pairs as shown in Fig. 1, Figure S4, and Table S1. The dominant peak of the Li–F pair at ca. 8 Å shown in Fig. 1a suggests that for 1.0 M LiPF$_6$ in EC, most of the LiPF$_6$ salt forms solvent separated ion pairs (SSIP), while the contact ion pairs (CIP) present as minority species (Fig. 2b). In addition, a trace amount (less than 1%) of aggregate solvates (AGG) were also observed during the simulation. By integrating the $g(r)$ to 3.0 Å, the total coordination number (CN) for Li ion is obtained as shown in Fig. 2a. Interestingly, while most of the first solvation shell is occupied by EC solvent molecules (5.84 out of 5.90) with a most probable distance of 2.08 Å to Li$^+$, the Li$^+$ solvation sheaths also present an average of 0.06 PF$_6^-$ anions, most of which form monodentate structures coordinated through a fluorine. The simulation produced a longer distance of 2.11 Å for the Li–F pair, illustrating that EC molecules take closer positions in solute complexes. The AGG species are rare, indicating an almost negligible number of Li ions that coordinate with more than one PF$_6^-$ anion. Hence, the corresponding CIP ratio is estimated as 6%, with a SSIP ratio of 94%, which agrees qualitatively with previous MD simulations [86], and is in agreement with common assumptions that LiPF$_6$ is a weakly co-ordinating salt compared to LiBF$_4$ and well dissociated in EC solutions [87].

Upon addition of 10% FEC into the LiPF$_6$/EC electrolyte, the solvation structure is evidently altered in several ways, primarily due to the weakened donor ability of FEC. Besides the similar solvation

structures as shown in Fig. 2b, other solute complex structures containing FEC were also observed in the snapshots of the MD simulation (Fig. 2c). Intriguingly, it is the carbonyl O in FEC that binds with the Li ion rather than F, which means that the composition difference of the solvent molecule does not radically alter the binding behavior as compared with the parent EC molecule [63]. However, the average CN for Li–O(EC) pair decreases from 5.84 to 5.51, allowing for an average Li–O(FEC) pair contribution of 0.19 to the first solvation shell. A maximum in $g(r)$ of 2.12 Å was observed for the Li–O(FEC) pair, suggesting a weaker interaction between Li-FEC as compared to Li-EC. Notably, the CIP ratio doubles from 6% to 14%, which significantly changes the statistics of the SEI formation reaction precursors, indicating a prominent role of FEC, even as a minority species. Similar to the EC electrolyte, the simulation with FEC additive results in a same Li-EC distance. Yet, the Li-FEC distance is slightly farther away (2.12 Å) as compared to the Li-EC counterparts, which results in a 'looser' structuring of the first solvation shell. EC electrolytes are known to promote salt dissociation due to its high dipole moment (5.64 Debye, calculated), as well as a high donor number. In contrast, FEC exhibits a lower dipole moment (4.97 Debye, calculated) which results in less dissociation of LiPF$_6$ and weakened donor ability (i.e. smaller CN of Li$^+$-solvent). This was further illustrated by inspecting the different charge population on the carbonyl oxygen of each molecule. Natural bond orbital analysis results in a charge on O$_{EC}$ of -0.66, while the charge on O$_{FEC}$ is -0.62, indicating the weaker donor ability of FEC as compared to EC. If we compare all six simulated compositions listed in Fig. 2a, it is obvious that a higher LiPF$_6$ concentration gives a higher CIP ratio. More importantly, when FEC is added to the system, a non-negligible percentage of the solute complexes are modified with fluorine-containing FEC that occupy the first solvation shell. The tendency for CIP formation can be represented by the free energy $\Delta_f G_{CIP}$ which is obtained through the CIP population, assuming a Boltzmann distribution of electrolyte species. Table 1 summarizes the results which show that higher salt concentration as well as inclusion of FEC reduces the energy cost of contact ion pairing. Previous first-principles calculations

SSIP

CIP

AGG

SSIP with 1 FEC

SSIP with 2 FEC

CIP with 1 FEC

AGG
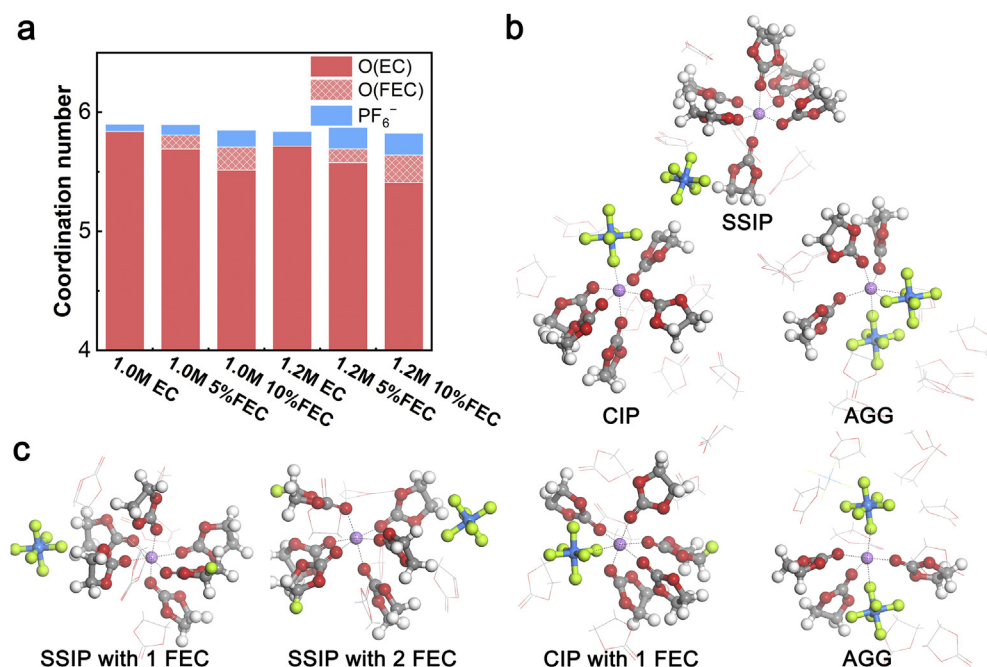
Fig. 2. (a)The calculated total coordination number for Li$^+$ in 1.0 M LiPF$_6$ in EC with 0/5/10% FEC and 1.2 M LiPF$_6$ in EC with 0/5/10% FEC with specifying the contributions from EC, FEC and PF$_6^-$. The representative solvation structures taken from MD simulation snapshots of (b) 1.0 M LiPF$_6$ in EC and (c) 1.0 M LiPF$_6$ in EC with 10% FEC. The carbon, hydrogen, oxygen, fluorine, phosphorus, and lithium elements are represented by grey, white, red, green, blue, and purple, respectively.

reported a $\Delta_f G_{CIP}$ of 2.6 kcal mol^{-1} for the Li$^+$ − (PC)$_4$ to Li$^+$ − PF$_6^-$ (PC)$_3$ conversion [88], which is approximately 1 kcal mol^{-1} higher than that of 1.0 M LiPF$_6$/EC obtained here from the CIP population. We speculate that the inclusion of explicit solvation effects beyond the first solvation shell as well as polarization effects not included in the current simulations may contribute to the difference between the two methodologies. In particular, the inclusion of 10% of FEC further reduces the solvating strength of the composite electrolyte, and allow for more CIPs, i.e. for PF$_6^-$ to directly contact/interact with Li$^+$. The coordination number for the Li-FEC pair increases to 0.2, which means that about 20% of the solvate structures on average now contain at least one FEC. We argue that this content change of the solute complex significantly changes the reduction potentials of the electrolyte constituents, which will be addressed further in the following sections. We also note that, with a higher temperature, the total coordination number of Li$^+$ is lower [89]. Therefore, a test of the electrolyte system under a sequential temperature of 330 K, 350 K, 400 K were performed to validate the results (Table S2). It was found that, with higher temperature, the CN for Li$^+$-EC decreases from 5.84 (298 K) to 5.23 (400 K), and the population of Li$^+$-PF$_6^-$ CIPs increases from 6% (298 K) to 25% (400 K). This may be explained by the increase in random thermal motion of solvent molecules resulting in a decrease of the dielectric constant and weakened EC-Li (dipole-charge) interactions. Thus, the Li-PF$_6^-$ (charge-charge) interaction would be gradually favored with elevated T.

4.2. Transport properties

Based on the mean square displacement (MSD) of each component during the simulation (Figure S5), the self-diffusion coefficients and transference numbers were calculated and plotted along with the reference experimental results [90] in Fig. 3. Both 1.0 M and 1.2 M simulation results indicate that the diffusion coefficients of all components within the EC electrolyte and EC/FEC mixture exhibit similar values (Fig. 3a). The trends for the three components EC, PF$_6^-$ and Li$^+$ are in good agreement with the simulation results [89] obtained by a generalized AMBER force field (GAFF) [91] as well as the trend from NMR results by Hayamizu et al. [90] such that solvent diffusivities are 2–5 × larger than ion diffusivities. While all the simulations predict slower computed dynamics than the experimental results, the difference is within one order of magnitude (10^{-10}–10^{-11} m^2 s^{-1}), illustrating that the classical MD simulation is adequately accurate to reproduce or predict the dynamical property trends of this system. It is noteworthy that, when FEC is added into the system, there is no significant variation of transport properties. EC and FEC exhibit almost the same diffusion coefficients within the numerical uncertainties and we surmise that the intermolecular interaction behaviors of EC and FEC are similar due to the common cyclic carbonyl structures with only one substituent. Hence, adding FEC does not *directly* affect the transport property of the electrolyte. On the other hand, FEC inclusion implicitly promotes the formation of CIPs while still remaining a minority species in the electrolyte. According to the Nernst–Einstein relation [92], an 8% CIP ratio increase from EC electrolyte to EC with 10% FEC will lead to

Table 1
The calculated coordination number of Li-X pairs, total coordination number, CIP ratio and corresponding contact ion pair (CIP) formation free energy $\Delta_f G_{CIP}$ of 1.0 M LiPF$_6$ in EC with 0/5/10% FEC and 1.2 M LiPF$_6$ in EC with 0/5/10% FEC.

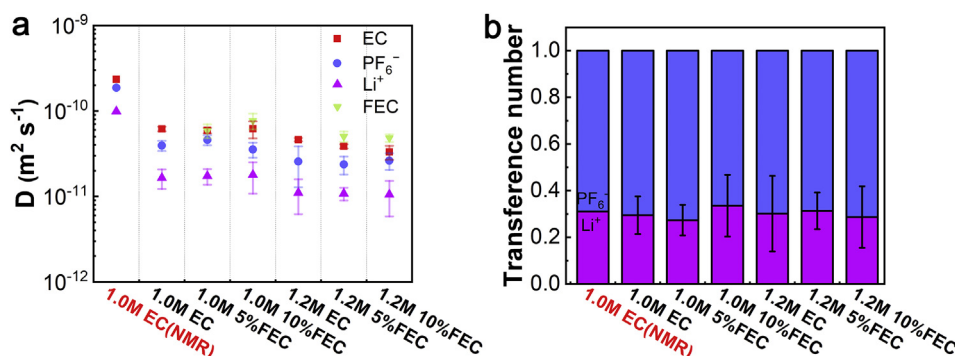| Electrolyte	Coordination number					CIP ratio	$\Delta_f G_{CIP}$ (kcal mol^{-1})
	O(EC)	O(FEC)	P(PF$_6^-$)	F(PF$_6^-$)	Total		
1.0 M EC	5.84	–	0.06	0.07	5.90	6%	1.63
1.0 M EC w/5%FEC	5.69	0.12	0.09	0.09	5.90	9%	1.37
1.0 M EC w/10%FEC	5.51	0.19	0.14	0.17	5.85	14%	1.07
1.2 M EC	5.71	–	0.12	0.20	5.84	12%	1.18
1.2 M EC w/5%FEC	5.58	0.12	0.18	0.20	5.87	18%	0.90
1.2 M EC w/10%FEC	5.41	0.23	0.18	0.23	5.82	18%	0.90

Fig. 3. (a) Self-diffusion coefficients computed from MD simulations at 298 K as compared with NMR experiments (1.0 M LiPF$_6$ in EC) from Hayamizu et al. [90] (b) Transference numbers for Li$^+$ and PF$_6^-$ from MD simulations and NMR experiments from Hayamizu et al. [90] The error bars represent the standard deviation of the data collected every 1 ns during the 5 ns production runs.

approximately the same percentage (8%) decrease in Li$^+$ ionic conductivity. In contrast, the salt concentration clearly affects the ionic diffusivity, decreasing by an average of ca. 30% from 1.0 to 1.2 M, in agreement with previous studies [86]. As for the transference number, all the six electrolyte systems give similar results and coincide well with the NMR experimental value of 0.35 [90]. Hence, both the self-diffusion coefficient and the transference number results demonstrate a weak dependence of transport properties on the FEC additive up to 10%, elucidating that FEC modifies the solvation structure without greatly affecting the ion transport ability.

4.3. FTIR measurements

In order to verify the theoretical simulation results, we conducted FTIR measurements for a range of EC and EC/FEC electrolytes [93]. The peaks from the FTIR spectrum are deliberately deconvoluted to quantitatively estimate the population proportion of each electrolyte species. In parallel, we performed quantum chemical calculations to obtain the theoretical IR vibrational information for each solvation structure observed in the MD simulations. The calculated spectral profiles are further linearly combined using the population ratios obtained from MD simulations which result in predicted theoretical IR spectra. In general, there are four major characteristic peaks [94] that are shifted after the inclusion of FEC (Figure S6): (1) the C=O stretching band at 1760–1800 cm^{-1}, (2) the C=O breathing band at 710–730 cm^{-1}, (3) the P–F stretching band at 840–880 cm^{-1}, as well as (4) the ring breathing band at 890–910 cm^{-1}. The C=O breathing vibrational band at 710–730 cm^{-1} can be used to distinguish the responses from different C=O binding states. Experimental peaks (Fig. 4a and 4b) were designated as coordinated and uncoordinated based on the calculations as well as reference data [94], which provide detailed information of the solvation structure. First, we note that the experimental results are in good agreement with the calculated spectra (Fig. 4c and d, and S7), and identical peaks are found in the spectra from both methods, despite small deviations in the absolute frequency values. For the EC electrolyte (Fig. 4a), two peaks at 728 cm^{-1} and 715 cm^{-1} were identified as coordinated EC and uncoordinated EC, both accompanied by a small C–H deformation peak at 706 cm^{-1} [95]. By analyzing the measured peak area integrals, it was found that 38.1% of EC molecules are coordinated with Li$^+$, which corresponds to a CN of 5.13 for Li-EC. While the calculated CN (5.84) from MD simulations is slightly higher than the experimental result, notably, both approaches indicate a CN over 5 for the EC electrolyte system. When 10% of FEC is included, an additional peak arises at 738 cm^{-1}, corresponding to the coordinated FEC. Meanwhile, a free FEC breathing band at 729 cm^{-1} overlaps with the coordinated EC vibration band (Fig. 4b), which makes it challenging to deconvolute the peaks and obtain the exact percentage of the coordinated EC and uncoordinated FEC. By comparing the peaks of the uncoordinated EC, we estimate an increase in uncoordinated EC area by 6.6% as compared to the 1 M LiPF$_6$ in EC system, further supporting the decrease in CN of Li$^+$-EC with respect to the EC electrolyte. Additionally, the CN of FEC

to Li$^+$ is directly calculated as 0.21 from the green area, which corresponds well with our previous calculation results (0.19) from the MD simulations.

In addition to the CN of solvents, the tendency for contact ion pairing was probed by analyzing the P–F bond stretching band. As shown in Fig. 5, the peak at 838–840 cm^{-1} is identified as the response from uncoordinated PF$_6^-$, while the two peaks at 878 cm^{-1} and 834 cm^{-1} arise through Li$^+$-coordinated PF$_6^-$. In the EC electrolyte (Fig. 5a), coordinated PF$_6^-$ contributes 6.4%, showing an excellent agreement with our simulated 6% CIP ratio. With the inclusion of FEC in the EC electrolyte (Fig. 5b), an FEC ring deformation vibration band appears at 862 cm^{-1}, which complicates the integral area calculation. By comparing the area change of the uncoordinated peak (Figure S8), we estimate that approximately 15% of the total PF$_6^-$ ions coordinate with Li$^+$ after adding FEC. In summary, both experimental and simulation results suggest that the CIP ratio, ca. 15% and 14% respectively, is increased under the influence of FEC additive.

The C=O bond stretching at 1790–1810 cm^{-1} is considered characteristic of the binding state of the carbonyl group [94]. However, an overtone peak of the ring breathing band appears at the same position in the same area (Figure S9) [95–97]. While the C=O stretching vibration is here calculated to be a single band at 1808 cm^{-1} by first-principles, experimentally, it overlaps with the Fermi resonance of an overtone of the ring in-plane breathing band (893 cm^{-1}). When solvent molecules coordinate to Li$^+$, both these peaks are shifted, preventing further meaningful interpretation. As for the ring breathing band at 893 cm^{-1}, a sharp, blue-shifted signal at 904 cm^{-1} appears upon coordination (Figure S10). The intensity of the shifted ring breathing band is significantly increased as compared to the original peak and hence prevents qualitative analysis. Consequently, due to these complexities, the C=O bond stretching and the ring breathing bands are disqualified for quantitatively analysis of the solvation structure. In summary, the FTIR experiments and the MD simulations provide consistent solvation structure information. Both approaches demonstrate that the LiPF$_6$/EC electrolyte with or without FEC results in a Li$^+$ CN of 5–6. We note that while carbonate-based electrolytes are traditionally believed to exhibit majority species corresponding to tetrahedrally coordinated carbonyl oxygen atoms around Li$^+$ [89,98,99], the coordination number and solvation structure in these solvents systems are still under debate [99]. Recent results have reported a CN of 5–6 from two-dimensional infrared spectroscopy [100], ^{13}C NMR [88,101], ^{17}O NMR [102], and MD simulation [86], in agreement with the results in this contribution. In contrast, several previous AIMD simulations [103–105] suggest tetrahedral Li$^+$-solvent coordination in the first coordination shell. However, we note that the typical simulation time in AIMD simulation (< 1 ns) is less than the residence time of a typical lithium-anion/solvent pair [106,107] and hence it may not capture the equilibrium state. In addition, Borodin et al. [106] also reported a coordination number of 4 for 1 M LiPF$_6$/EC using a polarizable force fields model. However, a very high contact ion pair ratio of 80% was also observed in the simulation, contrasting the perception of LiPF$_6$ as a weakly coordinating
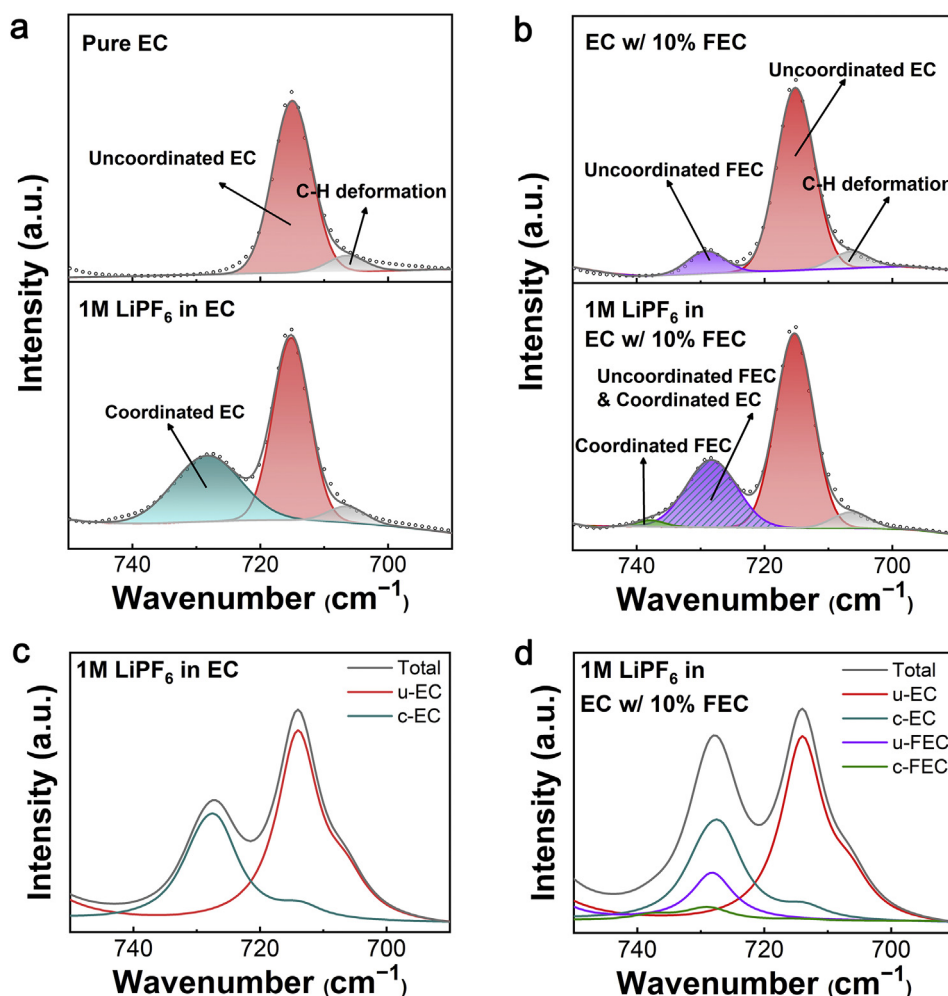
Fig. 4. Measured FTIR spectra of the C=O breathing band of (a) pure EC and 1.0 M LiPF$_6$ in EC, and (b) EC with 10% FEC and 1.0 M LiPF$_6$ in EC with 10% FEC. (c–d) The corresponding calculated IR spectra in comparison with the experimental results. Red, cyan, purple, green, grey and dark grey lines correspond to uncoordinated EC, EC coordinated with Li$^+$, uncoordinated FEC, FEC coordinated with Li$^+$, C–H deformation, and total spectrum, respectively. Scatter points denote the original FTIR data points.

salt [87].

Furthermore, our results conclusively suggest that adding FEC increases the CIP ratio while also adding another fluorine-containing species into the first solvation shell, without significantly impacting the transport properties of either Li$^+$ and PF$_6^-$ ions. This minority FEC coordination with Li$^+$ is important, as the Li$^+$ solvate complex serves as a key precursor for electrode surface reduction reactions. The inclusion of FEC in the first solvation shell, even as a minority species, increases the reduction potential of FEC, due to its close proximity of Li$^+$, as compared to a freely solvated FEC. Hence, to further investigate the critical influence of FEC on the SEI formation process, through the solvation structure of the electrolyte, we performed first-principles calculations of the reduction potential of the solvate structures obtained from the MD simulations and analyzed their preliminary reduction products.

4.4. Reduction potentials

The reduction potentials of free EC and FEC, their corresponding Li$^+$(solvent) complexes, and Li$^+$−PF$_6^-$ (solvent) complexes were investigated at the B3LYP/6–31 + g(d) level of theory (Table 2). To effectively compare with experimental results, the calculated potential values were convoluted with an arbitrary 0.1 V width concave triangular wave, and plotted together with the experimental differential capacity (dQ/dV) versus potential (V) profile (Fig. 6) [108]. The

reduction products after geometry optimization were further scrutinized through spin density analysis to elucidate the reduction reaction process (Fig. 7). The free EC molecule exhibits a calculated reduction potential of 0.21 V, with most of the extra electron residing on the O=CO(O) moiety which consequently deforms out of plane. According to Natural Bond Orbital (NBO) analysis, the C atom hybridization state changes from sp$^{2.0}$ to sp$^{2.6}$ to accommodate the extra e$^-$. The coordinated EC exhibits an increased reduction potential of 0.44 V–0.59 V (within 0.15 V), as compared with the uncoordinated molecule, which contributes to a broadening of the reduction peaks in the differential capacity plot. The obtained reduction potential is in good agreement with the previously obtained value of 0.53 V by G4MP2 [59]. Furthermore, the electron density of the reduced coordinated EC resides in the same region (e.g., on the O=CO(O)) as compared to the uncoordinated reduced EC. (Fig. 7c, h, i, k, and l). We find weak to little dependence of the reduction potential on the number of explicitly coordinating solvents [59,109], e.g., the calculated corresponding reduction potentials are 0.50 V and 0.59 V for 5- and 6- fold structures (Fig. 7k, and l), respectively. However, when Li$^+$ is in direct coordination with FEC, the predicted FEC reduction potential is obtained as 0.81 V–0. 91 V, which is about 0.3 V higher than uncoordinated FEC. The calculated reduction potentials are in good agreement with the previous G4MP2 calculations (0.90 V) and measured values (1.0 V) [110]. If we compare the reduction behavior of EC-containing species and FEC-containing species, even the uncoordinated FEC exhibits an
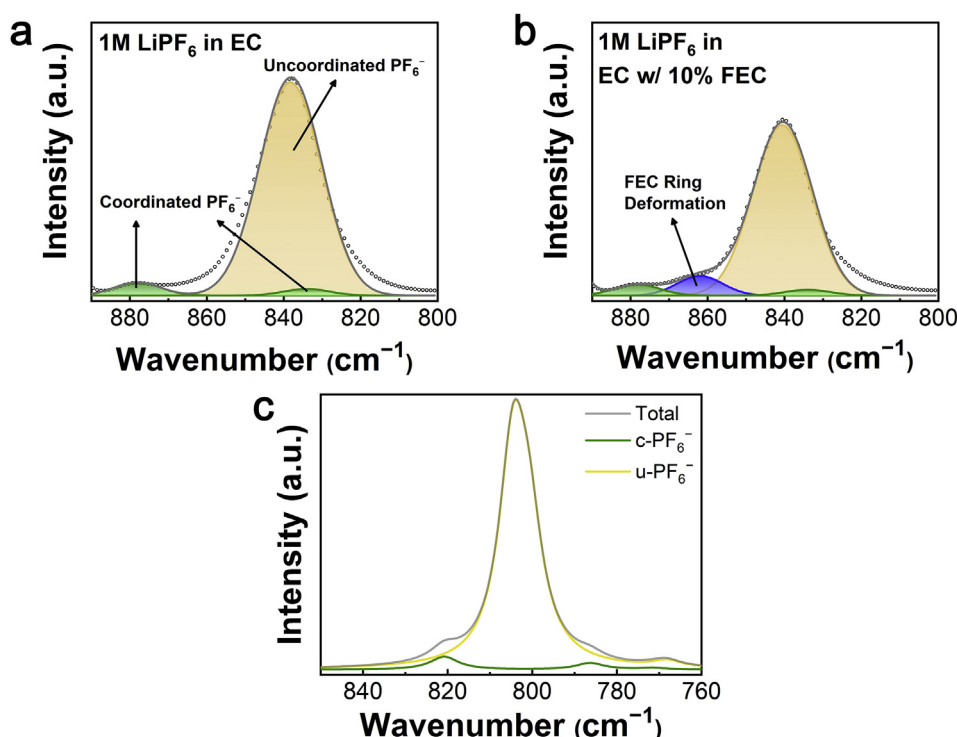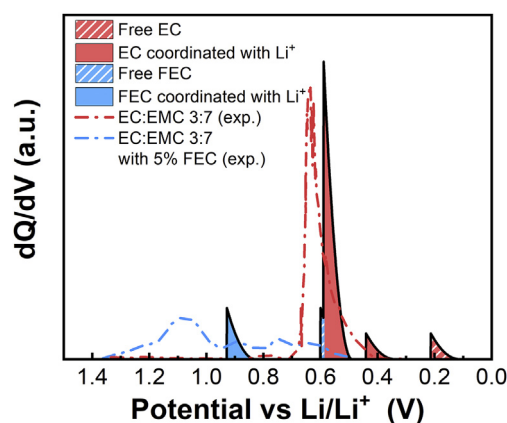
Fig. 5. Measured FTIR spectra of the P–F bond stretching band of (a) 1.0 M LiPF$_6$ in EC, and (b) 1.0 M LiPF$_6$ in EC with 10% FEC. (c) The corresponding calculated IR spectra for 1.0 M LiPF$_6$ in EC in comparison with the experimental results. Yellow, green, blue, and dark grey lines correspond to uncoordinated PF$_6^-$, coordinated PF$_6^-$, FEC ring deformation, and total spectrum, respectively. Scatter points denote the original FTIR data points.

Table 2

The reduction potential vs Li + /Li(s) (i.e. subtract 1.4 V) of individual solvent molecules and solvate complexes, in Volt, where *corr.* denotes values after the aforementioned standard-state correction.

| Structures	Reduction potential
EC + e$^-$ → EC$^-$	0.21 V
FEC + e$^-$ → FEC$^-$	0.59 V
Li$^+$ − EC + e$^-$ → Li$^+$ − (EC)$^-$	0.54 V
Li$^+$ − FEC + e$^-$ → Li$^+$ − (FEC)$^-$	0.90 V
Li$^+$ − (EC)$_4$ + e$^-$ → Li$^+$ − (EC)$_3$(EC)$^-$	0.49 V
Li$^+$ − (EC)$_3$(FEC) + e$^-$ → Li$^+$ − (EC)$_2$(FEC)(EC)$^-$	0.55 V
Li$^+$ − (EC)$_3$(FEC) + e$^-$ → Li$^+$ − (EC)$_3$(FEC)$^-$	0.91 V
Li$^+$ − (EC)$_5$ + e$^-$ → Li$^+$ − (EC)$_3$(EC)$^-$ + EC	0.50 V (corr.)
Li$^+$ − (EC)$_6$ + e$^-$ → Li$^+$ − (EC)$_3$(EC)$^-$ + 2EC	0.59 V (corr.)
Li$^+$ − (EC)$_5$(FEC) + e$^-$ → Li$^+$ − (EC)$_3$(FEC)$^-$ + 2EC	0.81 V (corr.)
Li$^+$ − PF$_6^-$ + e$^-$ → Li$^+$ − F$^-$ + PF$_5^-$	spontaneous bond breaking
Li$^+$ − PF$_6^-$(EC) + e$^-$ → Li$^+$ − PF$_6^-$(EC) $^-$	0.59 V
Li$^+$ − PF$_6^-$(FEC) + e$^-$ → Li$^+$ − PF$_6^-$(FEC) $^-$	0.90 V
Li$^+$ − PF$_6^-$(EC)$_5$ + e$^-$ → Li$^+$ − (EC)$_3$(EC)$^-$ + PF$_6^-$ + EC	0.44 V (corr.)

Fig. 6. The calculated anticipated (solid line) and experimental (dash dotted line) differential capacity plots (dQ/dV vs. V) during the formation step of EC and FEC electrolyte. The computed profile is obtained by convoluting the calculated reduction potentials with a 0.1 V width concave triangular wave, the experimental one is reproduced from Xia et al. [108] by removing the background.

equal or higher reduction potential than all investigated EC species, indicating a preferential reduction for FEC vs EC—for both minority as well as majority species. While the optimized FEC reduction products (Fig. 7b, d, j, and m) exhibit the same electron distributions as its EC counterparts, the stronger exothermic nature of the FEC reduction indicates that these FEC-derivative species are sufficiently metastable to decay through reactions other than the C–O bond ring-opening of EC [27]. This major mechanistic difference between the non-fluorinated and fluorinated carbonates allows for the recombination of fragments and intramolecular electron migration, facilitating the subsequent polymerization and LiF formation [27]. Previous DFT calculations have shown that the additional F fragments from FEC decomposition exhibit a "glue effect" by strongly binding to Li atoms of multiple organic species and connecting them [63], leading to a more compact and stable SEI. The formation of Li$^+$-coordinated FEC species is especially important because in their absence, there is no early onset FEC reduction. Indeed, uncoordinated FEC is predicted to reduce at a similar

potential as Li + coordinated EC, which, as the majority solvent, will then dominate the SEI formation process. We also note that, as Li$^+$-coordinated FEC minority species are decomposing at higher potentials, the bulk equilibrium will shift to maintain the population, hence supplying the reaction.
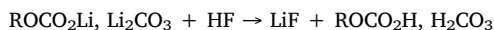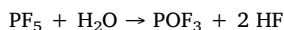
The reduction of the Li$^+$ − PF$_6^-$ contact ion pair results in direct LiF formation. Upon geometry optimization, the PF$_6^-$ structure is dynamically unstable, and the P–F bond spontaneously breaks to form PF$_5^-$ and LiF (Fig. 7e). However, the Li$^+$ − PF$_6^-$ ion pair decomposition is expected to yield high reaction barrier at potential larger than 0.5 V [111]. When explicit solvent molecules are considered in the contact ion pair model, the reduction of the complex results in solvent reduction, elucidating that the decomposition of solvent molecules are preferred over that of the ion-paired PF$_6^-$ (Fig. 7f, g, and n), with similar reduction potential as SSIP structures. Thus, FEC will be reduced before
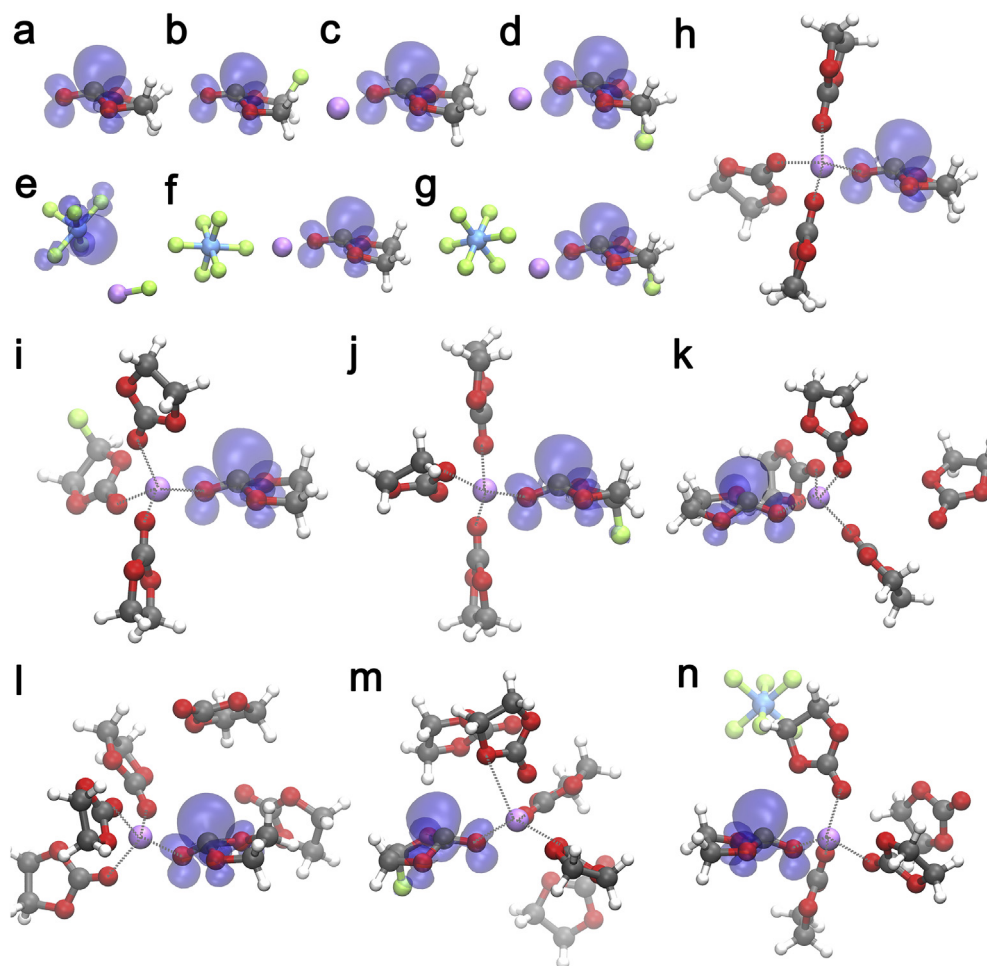
Fig. 7. Geometries and spin density analysis of reduced solvent molecules (a) EC, (b) FEC, and solvate complexes (c) Li^+-EC, (d) Li^+-FEC, (e) $Li^+-PF_6^-$, (f) $Li^+-PF_6^-(EC)$, (g) $Li^+-PF_6^-(FEC)$, (h) $Li^+-(EC)_4$, (i) $Li^+-(EC)_3(FEC)$ (EC reduction), (j) $Li^+-(EC)_3(FEC)$ (FEC reduction), (k) $Li^+-(EC)_5$, (l) $Li^+-(EC)_6$, (m) $Li^+-(EC)_5(FEC)$ (FEC reduction), and (n) $Li^+-PF_6^-(EC)_5$.

other species considered here. The reduction of PF_6^- is not expected to occur except at very high overpotentials, possibly at the final stage of SEI formation [111]. Therefore, we suggest that FEC is the major contributor to the formation of the SEI LiF as compared to PF_6^-. It is also speculated that the decomposition of PF_6^- is related to H_2O contamination rather than electrochemical reactions [52]. The degradation mechanism for $LiPF_6$ was suggested to be [112]:

$$LiPF_6 \leftrightarrow LiF + PF_5$$

$$PF_5 + H_2O \rightarrow POF_3 + 2\ HF$$

$$ROCO_2Li,\ Li_2CO_3 + HF \rightarrow LiF + ROCO_2H,\ H_2CO_3$$
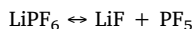
On one hand, a higher CIP ratio in the presence of FEC would facilitate the formation of LiF. Increased amount of $Li^+-PF_6^-$ ion pairs would promote PF_5 formation and pronounced hydrolysis, and the as-formed HF would subsequently react with the SEI carbonate species, which are initial reduction products, to form LiF [113]. Even if the trace amount of water is ignored, FEC is prone to defluorination in the presence of a Lewis acid like PF_5, and subsequently generates F species [114]. Consequently, a greater amount of inorganic components in SEI, introduced by the sacrificial anion decomposition [115,116] or FEC defluorination, is believed to result in improved Li^+ cation transport. However, excessive HF formation under elevated temperatures may also cause SEI destruction [114], such that the operating temperature of the FEC-containing electrolyte should be controlled to avoid detrimental effect. On the other hand, an early onset of FEC reduction allows

for rapid passivation at a higher potential than EC which may limit PF_6^- reduction/decomposition. Therefore, the influence of FEC on PF_6^- decomposition is non-trivial to deconvolute. Future experimental and computational research, e.g. isotopic labelling, is recommended.

In summary, despite limited FEC concentration, we find that its presence significantly influences the properties of the electrolyte via three main mechanisms: (i) the Li^+-coordinated FEC exhibits higher reduction potential than corresponding coordinated EC species and uncoordinated FEC, and hence contributes to an early onset of anode SEI formation and passivation, and (ii) the preferred reduction of FEC introduces a higher ratio of LiF to the SEI as compared to the EC equivalent electrolyte, and lastly (iii) a higher CIP ratio may possibly lead to increased LiF formation. The exothermic nature of the FEC reduction also supports the reported reaction pathway of defluorination and subsequent polymerization. Therefore, the origin of the excellent performance of FEC containing electrolyte may be attributed to the higher reduction potential to enable early passivation [117], substituents that promotes inorganic product formation [118], and metastable intermediates to facilitate alternative reaction pathways (such as polymerization) [27,35].

5. Conclusions

The influence of FEC on $LiPF_6$/EC electrolytes is investigated through classical MD simulations, FTIR experiments and first-principles calculations. The calculated solvation structure corroborates well with

the liquid structure information inferred by experiments. While select previous work advocate Li$^+$ coordination numbers closer to 4, both theoretical and experimental results presented here support a Li$^+$ solvent coordination number of 5–6 for 1.0/1.2 M LiPF$_6$/EC electrolytes, with or without FEC. However, reduction potentials are found to exhibit only weak dependence on the explicit number of coordinating solvents, such that 4-fold as well as 6-fold structures show similar values. Furthermore, while it is widely assumed that electrolyte additives remain largely uncoordinated in LIB electrolytes, we find that FEC, as a minority species, significantly modifies the solvation structure and reduction behavior of the electrolyte while being innocuous to the transport properties of the electrolyte. Even limited 5–10% addition of FEC results in a notably higher CIP ratio (14%, 1.0 M EC w/10% FEC) as compared to the parent EC electrolyte (6%, 1.0 M EC). FEC itself, as a fluorine-containing species, appears in the solvate complex, in 19% of the Li$^+$ first solvation shells (1.0 M EC w/10%FEC). We find that the Li$^+$-coordinated FEC is preferentially reduced at higher reduction potentials (about 0.3 V higher than corresponding EC clusters and uncoordinated FEC), which provides early onset SEI formation and passivation of the anode surface. Meanwhile, the as-formed reduction products of FEC include a higher ratio of LiF as compared to the EC equivalent electrolyte, and a higher CIP ratio due to FEC addition may further benefit LiF formation, leading to enhanced electrochemical performance. By elucidating the solvation structure of the FEC additive in LiPF$_6$/EC, and its effect on the reduction potentials of the composite electrolyte, we hope to improve our understanding of the SEI-formation and its subtle dependence on the detailed intermolecular interactions and resulting solvation structure of the electrolyte.

Conflicts of interest

There are no conflicts of interest to declare.

Acknowledgements

Appendix A. Supplementary data

Supplementary data to this article can be found online at https://doi.org/10.1016/j.nanoen.2019.103881.

References

[1] X. Chen, X. Shen, B. Li, H.J. Peng, X.B. Cheng, B.Q. Li, X.Q. Zhang, J.Q. Huang, Q. Zhang, Ion-solvent complexes promote gas evolution from electrolytes on a sodium metal anode, Angew Chem. Int. Ed. Engl. 57 (2018) 734–737 https://doi.org/10.1002/anie.201711552.

[2] X.Q. Zhang, X. Chen, X.B. Cheng, B.Q. Li, X. Shen, C. Yan, J.Q. Huang, Q. Zhang, Highly stable lithium metal batteries enabled by regulating the solvation of lithium ions in nonaqueous electrolytes, Angew Chem. Int. Ed. Engl. 57 (2018) 5301–5305 https://doi.org/10.1002/anie.201801513.

[3] B. Liu, W. Xu, P. Yan, S.T. Kim, M.H. Engelhard, X. Sun, D. Mei, J. Cho, C.-M. Wang, J.-G. Zhang, Stabilization of Li metal anode in DMSO-based electrolytes via optimization of salt-solvent coordination for Li-O2 batteries, Adv. Energy Mater. 7 (2017) 1602605 https://doi.org/10.1002/aenm.201602605.

[4] K. Schroder, J. Alvarado, T.A. Yersak, J. Li, N. Dudney, L.J. Webb, Y.S. Meng, K.J. Stevenson, The effect of fluoroethylene carbonate as an additive on the solid electrolyte interphase on silicon lithium-ion electrodes, Chem. Mater. 27 (2015) 5531–5542 https://doi.org/10.1021/acs.chemmater.5b01627.

[5] X.-B. Cheng, C. Yan, X. Chen, C. Guan, J.-Q. Huang, H.-J. Peng, R. Zhang, S.-T. Yang, Q. Zhang, Implantable solid electrolyte interphase in lithium-metal batteries, Chem 2 (2017) 258–270 https://doi.org/10.1016/j.chempr.2017.01.003.

[6] S. Shi, P. Lu, Z. Liu, Y. Qi, L.G. Hector Jr., H. Li, S.J. Harris, Direct calculation of Li-ion transport in the solid electrolyte interphase, J. Am. Chem. Soc. 134 (2012) 15476–15487 https://doi.org/10.1021/ja305366r.

[7] S. Shi, Y. Qi, H. Li, L.G. Hector, Defect thermodynamics and diffusion mechanisms in Li2CO3 and implications for the solid electrolyte interphase in Li-ion batteries, J. Phys. Chem. C 117 (2013) 8579–8593 https://doi.org/10.1021/jp310591u.

[8] D. Aurbach, The study of electrolyte solutions based on ethylene and diethyl carbonates for rechargeable Li batteries, J. Electrochem. Soc. 142 (1995), https://doi.org/10.1149/1.2048658.

[9] K. Xu, Y. Lam, S.S. Zhang, T.R. Jow, T.B. Curtis, Solvation sheath of Li + in nonaqueous electrolytes and its implication of graphite/electrolyte interface chemistry, J. Phys. Chem. C 111 (2007) 7411–7421 https://doi.org/10.1021/jp068691u.

[10] D.M. Seo, D. Chalasani, B.S. Parimalam, R. Kadam, M. Nie, B.L. Lucht, Reduction reactions of carbonate solvents for lithium ion batteries, ECS Electrochem. Lett. 3 (2014) A91–A93 https://doi.org/10.1149/2.0021409eel.

[11] B. Philippe, R. Dedryvère, M. Gorgoi, H. Rensmo, D. Gonbeau, K. Edström, Role of the LiPF6 salt for the long-term stability of silicon electrodes in Li-ion batteries – a photoelectron spectroscopy study, Chem. Mater. 25 (2013) 394–404 https://doi.org/10.1021/cm303399v.

[12] T. Yoon, M.S. Milien, B.S. Parimalam, B.L. Lucht, Thermal decomposition of the solid electrolyte interphase (SEI) on silicon electrodes for lithium ion batteries, Chem. Mater. 29 (2017) 3237–3245 https://doi.org/10.1021/acs.chemmater.7b00454.

[13] B.S. Parimalam, A.D. MacIntosh, R. Kadam, B.L. Lucht, Decomposition reactions of anode solid electrolyte interphase (SEI) components with LiPF6, J. Phys. Chem. C 121 (2017) 22733–22738 https://doi.org/10.1021/acs.jpcc.7b08433.

[14] S. Jurng, Z.L. Brown, J. Kim, B.L. Lucht, Effect of electrolyte on the nanostructure of the solid electrolyte interphase (SEI) and performance of lithium metal anodes, Energy Environ. Sci. 11 (2018) 2600–2608 https://doi.org/10.1039/c8ee00364e.

[15] V. Etacheri, R. Marom, R. Elazari, G. Salitra, D. Aurbach, Challenges in the development of advanced Li-ion batteries: a review, Energy Environ. Sci. 4 (2011) 3243 https://doi.org/10.1039/c1ee01598b.

[16] X. Chen, X. Li, D. Mei, J. Feng, M.Y. Hu, J. Hu, M. Engelhard, J. Zheng, W. Xu, J. Xiao, J. Liu, J.-G. Zhang, Reduction mechanism of fluoroethylene carbonate for stable solid-electrolyte interphase film on silicon anode, ChemSusChem 7 (2014) 549–554 https://doi.org/10.1002/cssc.201300770.

[17] K. Xu, Nonaqueous liquid electrolytes for lithium-based rechargeable batteries, Chem. Rev. 104 (2004) 4303–4418 https://doi.org/10.1021/cr030203g.

[18] K. Xu, Electrolytes and interphases in Li-ion batteries and beyond, Chem. Rev. 114 (2014) 11503–11618 https://doi.org/10.1021/cr500003w.

[19] C. Xu, F. Lindgren, B. Philippe, M. Gorgoi, F. Björefors, K. Edström, T. Gustafsson, Improved performance of the silicon anode for Li-ion batteries: understanding the surface modification mechanism of fluoroethylene carbonate as an effective electrolyte additive, Chem. Mater. 27 (2015) 2591–2599 https://doi.org/10.1021/acs.chemmater.5b00339.

[20] H. Wu, G. Zheng, N. Liu, T.J. Carney, Y. Yang, Y. Cui, Engineering empty space between Si nanoparticles for lithium-ion battery anodes, Nano Lett. 12 (2012) 904–909 https://doi.org/10.1021/nl203967r.

[21] Y. Jin, S. Li, A. Kushima, X. Zheng, Y. Sun, J. Xie, J. Sun, W. Xue, G. Zhou, J. Wu, F. Shi, R. Zhang, Z. Zhu, K. So, Y. Cui, J. Li, Self-healing SEI enables full-cell cycling of a silicon-majority anode with a coulombic efficiency exceeding 99.9%, Energy Environ. Sci. 10 (2017) 580–592 https://doi.org/10.1039/c6ee02685k.

[22] C.C. Nguyen, T. Yoon, D.M. Seo, P. Guduru, B.L. Lucht, Systematic investigation of binders for silicon anodes: interactions of binder with silicon particles and electrolytes and effects of binders on solid electrolyte interphase formation, ACS Appl. Mater. Interfaces 8 (2016) 12211–12220 https://doi.org/10.1021/acsami.6b03357.

[23] C.C. Nguyen, D.M. Seo, K. Chandrasiri, B.L. Lucht, Improved cycling performance of a Si nanoparticle anode utilizing citric acid as a surface-modifying agent, Langmuir 33 (2017) 9254–9261 https://doi.org/10.1021/acs.langmuir.6b04310.

[24] Z. Chen, C. Wang, J. Lopez, Z. Lu, Y. Cui, Z. Bao, High-areal-capacity silicon electrodes with low-cost silicon particles based on spatial control of self-healing binder, Adv. Energy Mater. 5 (2015) 1401826 https://doi.org/10.1002/aenm.201401826.

[25] C.C. Nguyen, B.L. Lucht, Comparative study of fluoroethylene carbonate and vinylene carbonate for silicon anodes in lithium ion batteries, J. Electrochem. Soc. 161 (2014) A1933–A1938 https://doi.org/10.1149/2.0731412jes.

[26] B. Philippe, R. Dedryvere, M. Gorgoi, H. Rensmo, D. Gonbeau, K. Edstrom, Improved performances of nanosilicon electrodes using the salt LiFSI: a photoelectron spectroscopy study, J. Am. Chem. Soc. 135 (2013) 9829–9842 https://doi.org/10.1021/ja403082s.

[27] I.A. Shkrob, J.F. Wishart, D.P. Abraham, What makes fluoroethylene carbonate different? J. Phys. Chem. C 119 (2015) 14954–14964 https://doi.org/10.1021/acs.jpcc.5b03591.

[28] X.-Q. Zhang, X.-B. Cheng, X. Chen, C. Yan, Q. Zhang, Fluoroethylene carbonate additives to render uniform Li deposits in lithium metal batteries, Adv. Funct. Mater. 27 (2017) 1605989 https://doi.org/10.1002/adfm.201605989.

[29] M. Sina, J. Alvarado, H. Shobukawa, C. Alexander, V. Manichev, L. Feldman, T. Gustafsson, K.J. Stevenson, Y.S. Meng, Direct visualization of the solid electrolyte interphase and its effects on silicon electrochemical performance, Adv. Mater. Interfaces 3 (2016) 1600438 https://doi.org/10.1002/admi.201600438.

[30] F. Shi, P.N. Ross, G.A. Somorjai, K. Komvopoulos, The chemistry of electrolyte

reduction on silicon electrodes revealed by in situ ATR-FTIR spectroscopy, J. Phys. Chem. C 121 (2017) 14476–14483 https://doi.org/10.1021/acs.jpcc.7b04132.

[31] K.W. Schroder, H. Celio, L.J. Webb, K.J. Stevenson, Examining solid electrolyte interphase formation on crystalline silicon electrodes: influence of electrochemical preparation and ambient exposure conditions, J. Phys. Chem. C 116 (2012) 19737–19747 https://doi.org/10.1021/jp307372m.

[32] B. Breitung, P. Baumann, H. Sommer, J. Janek, T. Brezesinski, In situ and operando atomic force microscopy of high-capacity nano-silicon based electrodes for lithium-ion batteries, Nanoscale 8 (2016) 14048–14056 https://doi.org/10.1039/c6nr03575b.

[33] I. Yoon, D.P. Abraham, B.L. Lucht, A.F. Bower, P.R. Guduru, In situ measurement of solid electrolyte interphase evolution on silicon anodes using atomic force microscopy, Adv. Energy Mater. 6 (2016) 1600099 https://doi.org/10.1002/aenm.201600099.

[34] B.T. Young, D.R. Heskett, C.C. Nguyen, M. Nie, J.C. Woicik, B.L. Lucht, Hard X-ray photoelectron spectroscopy (HAXPES) investigation of the silicon solid electrolyte interphase (SEI) in lithium-ion batteries, ACS Appl. Mater. Interfaces 7 (2015) 20004–20011 https://doi.org/10.1021/acsami.5b04845.

[35] Y. Jin, N.H. Kneusels, P. Magusin, G. Kim, E. Castillo-Martinez, L.E. Marbella, R.N. Kerber, D.J. Howe, S. Paul, T. Liu, C.P. Grey, Identifying the structural basis for the increased stability of the solid electrolyte interphase formed on silicon with the additive fluoroethylene carbonate, J. Am. Chem. Soc. 139 (2017) 14992–15004 https://doi.org/10.1021/jacs.7b06834.

[36] A. Schiele, B. Breitung, T. Hatsukade, B.B. Berkes, P. Hartmann, J. Janek, T. Brezesinski, The critical role of fluoroethylene carbonate in the gassing of silicon anodes for lithium-ion batteries, ACS Energy Lett. 2 (2017) 2228–2233 https://doi.org/10.1021/acsenergylett.7b00619.

[37] Y. Zhang, M. Su, X. Yu, Y. Zhou, J. Wang, R. Cao, W. Xu, C. Wang, D.R. Baer, O. Borodin, K. Xu, Y. Wang, X.L. Wang, Z. Xu, F. Wang, Z. Zhu, Investigation of ion-solvent interactions in nonaqueous electrolytes using in situ liquid SIMS, Anal. Chem. 90 (2018) 3341–3348 https://doi.org/10.1021/acs.analchem.7b04921.

[38] C. Stetson, T. Yoon, J. Coyle, W. Nemeth, M. Young, A. Norman, S. Pylypenko, C. Ban, C.-S. Jiang, M. Al-Jassim, A. Burrell, Three-dimensional electronic resistivity mapping of solid electrolyte interphase on Si anode materials, Nano Energy, https://doi.org/10.1016/j.nanoen.2018.11.007.

[39] H. Shobukawa, J. Alvarado, Y. Yang, Y.S. Meng, Electrochemical performance and interfacial investigation on Si composite anode for lithium ion batteries in full cell, J. Power Sources 359 (2017) 173–181 https://doi.org/10.1016/j.jpowsour.2017.05.044.

[40] E. Markevich, G. Salitra, D. Aurbach, Fluoroethylene carbonate as an important component for the formation of an effective solid electrolyte interphase on anodes and cathodes for advanced Li-ion batteries, ACS Energy Lett. 2 (2017) 1337–1345 https://doi.org/10.1021/acsenergylett.7b00163.

[41] S. Shi, J. Gao, Y. Liu, Y. Zhao, Q. Wu, W. Ju, C. Ouyang, R. Xiao, Multi-scale computation methods: their applications in lithium-ion battery research and development, Chin. Phys. B 25 (2016), https://doi.org/10.1088/1674-1056/25/1/018212.

[42] A.L. Michan, B.S. Parimalam, M. Leskes, R.N. Kerber, T. Yoon, C.P. Grey, B.L. Lucht, Fluoroethylene carbonate and vinylene carbonate reduction: understanding lithium-ion battery electrolyte additives and solid electrolyte interphase formation, Chem. Mater. 28 (2016) 8149–8159 https://doi.org/10.1021/acs.chemmater.6b02282.

[43] B.S. Parimalam, B.L. Lucht, Reduction reactions of electrolyte salts for lithium ion batteries: LiPF6, LiBF4, LiDFOB, LiBOB, and LiTFSI, J. Electrochem. Soc. 165 (2018) A251–A255 https://doi.org/10.1149/2.0901802jes.

[44] C.D. Malliakas, K. Leung, K.Z. Pupek, I.A. Shkrob, D.P. Abraham, Spontaneous aggregation of lithium ion coordination polymers in fluorinated electrolytes for high-voltage batteries, Phys. Chem. Chem. Phys. 18 (2016) 10846–10849 https://doi.org/10.1039/c6cp01157h.

[45] S. Perez-Beltran, G.E. Ramírez-Caballero, P.B. Balbuena, First-principles calculations of lithiation of a hydroxylated surface of amorphous silicon dioxide, J. Phys. Chem. C 119 (2015) 16424–16431 https://doi.org/10.1021/acs.jpcc.5b02992.

[46] F.A. Soto, Y. Ma, J.M. Martinez de la Hoz, J.M. Seminario, P.B. Balbuena, formation and growth mechanisms of solid-electrolyte interphase layers in rechargeable batteries, Chem. Mater. 27 (2015) 7990–8000 https://doi.org/10.1021/acs.chemmater.5b03358.

[47] F.A. Soto, J.M. Martinez de la Hoz, J.M. Seminario, P.B. Balbuena, Modeling solid-electrolyte interfacial phenomena in silicon anodes, Curr. Opin. Chem. Eng. 13 (2016) 179–185 https://doi.org/10.1016/j.coche.2016.08.017.

[48] S.A. Delp, O. Borodin, M. Olguin, C.G. Eisner, J.L. Allen, T.R. Jow, Importance of reduction and oxidation stability of high voltage electrolytes and additives, Electrochim. Acta 209 (2016) 498–510 https://doi.org/10.1016/j.electacta.2016.05.100.

[49] J.M. Martinez de la Hoz, F.A. Soto, P.B. Balbuena, Effect of the electrolyte composition on SEI reactions at Si anodes of Li-ion batteries, J. Phys. Chem. C 119 (2015) 7060–7068 https://doi.org/10.1021/acs.jpcc.5b01228.

[50] J.M. Martinez de la Hoz, K. Leung, P.B. Balbuena, Reduction mechanisms of ethylene carbonate on si anodes of lithium-ion batteries: effects of degree of lithiation and nature of exposed surface, ACS Appl. Mater. Interfaces 5 (2013) 13457–13465 https://doi.org/10.1021/am404365r.

[51] J.M. Martinez de la Hoz, P.B. Balbuena, Reduction mechanisms of additives on Si anodes of Li-ion batteries, Phys. Chem. Chem. Phys. 16 (2014) 17091–17098 https://doi.org/10.1039/c4cp01948b.

[52] K. Leung, S.B. Rempe, M.E. Foster, Y. Ma, J.M. Martinez del la Hoz, N. Sai, P.B. Balbuena, Modeling electrochemical decomposition of fluoroethylene carbonate on silicon anode surfaces in lithium ion batteries, J. Electrochem. Soc. 161

(2013) A213–A221 https://doi.org/10.1149/2.092401jes.

[53] S. Perez-Beltran, G.E. Ramírez-Caballero, P.B. Balbuena, Ethylene carbonate reduction on lithiated surfaces of hydroxylated amorphous silicon dioxide, J. Electrochem. Soc. 163 (2016) A2197–A2202 https://doi.org/10.1149/2.0371610jes.

[54] K. Leung, Two-electron reduction of ethylene carbonate: a quantum chemistry reexamination of mechanisms, Chem. Phys. Lett. 568–569 (2013) 1–8 https://doi.org/10.1016/j.cplett.2012.08.022.

[55] S.J. An, J. Li, C. Daniel, D. Mohanty, S. Nagpure, D.L. Wood, The state of understanding of the lithium-ion-battery graphite solid electrolyte interphase (SEI) and its relationship to formation cycling, Carbon 105 (2016) 52–76 https://doi.org/10.1016/j.carbon.2016.04.008.

[56] S.E. Burkhardt, Impact of chemical follow-up reactions for lithium ion electrolytes: generation of nucleophilic species, solid electrolyte interphase, and gas formation, J. Electrochem. Soc. 164 (2017) A684–A690 https://doi.org/10.1149/2.0621704jes.

[57] F.A. Soto, P.B. Balbuena, Elucidating oligomer-surface and oligomer-oligomer interactions at a lithiated silicon surface, Electrochim. Acta 220 (2016) 312–321 https://doi.org/10.1016/j.electacta.2016.10.082.

[58] L. Benitez, D. Cristancho, J.M. Seminario, J.M. Martinez de la Hoz, P.B. Balbuena, Electron transfer through solid-electrolyte-interphase layers formed on Si anodes of Li-ion batteries, Electrochim. Acta 140 (2014) 250–257 https://doi.org/10.1016/j.electacta.2014.05.018.

[59] O. Borodin, X. Ren, J. Vatamanu, A. von Wald Cresce, J. Knap, K. Xu, Modeling insight into battery electrolyte electrochemical stability and interfacial structure, Acc. Chem. Res. 50 (2017) 2886–2894 https://doi.org/10.1021/acs.accounts.7b00486.

[60] Y. Ma, P.B. Balbuena, DFT study of reduction mechanisms of ethylene carbonate and fluoroethylene carbonate on Li+-Adsorbed Si clusters, J. Electrochem. Soc. 161 (2014) E3097–E3109 https://doi.org/10.1149/2.014408jes.

[61] A. Wang, S. Kadam, H. Li, S. Shi, Y. Qi, Review on modeling of the anode solid electrolyte interphase (SEI) for lithium-ion batteries, npj Comput. Mater. 4 (2018), https://doi.org/10.1038/s41524-018-0064-0.

[62] N. Takenaka, H. Sakai, Y. Suzuki, P. Uppula, M. Nagaoka, A computational chemical insight into microscopic additive effect on solid electrolyte interphase film formation in sodium-ion batteries: suppression of unstable film growth by intact fluoroethylene carbonate, J. Phys. Chem. C 119 (2015) 18046–18055 https://doi.org/10.1021/acs.jpcc.5b04206.

[63] Y. Okuno, K. Ushirogata, K. Sodeyama, Y. Tateyama, Decomposition of the fluoroethylene carbonate additive and the glue effect of lithium fluoride products for the solid electrolyte interphase: an ab initio study, Phys. Chem. Chem. Phys. 18 (2016) 8643–8653 https://doi.org/10.1039/c5cp07583a.

[64] S. Plimpton, Fast parallel algorithms for short-range molecular-dynamics, J. Comput. Phys. 117 (1995) 1–19 https://doi.org/10.1006/jcph.1995.1039.

[65] A. von Cresce, K. Xu, Preferential solvation of Li+ directs formation of interphase on graphitic anode, Electrochem. Solid State Lett. 14 (2011) A154–A156 https://doi.org/10.1149/1.3615828.

[66] L. Martinez, R. Andrade, E.G. Birgin, J.M. Martinez, PACKMOL: a package for building initial configurations for molecular dynamics simulations, J. Comput. Chem. 30 (2009) 2157–2164 https://doi.org/10.1002/jcc.21224.

[67] D.M. Seo, J.L. Allen, L.A. Gardner, S.D. Han, P.D. Boyle, W.A. Henderson, Electrolyte solvation and ionic association: cyclic carbonate and ester-LiTFSI and -LiPF6 mixtures, ECS Trans. 50 (2013) 375–380 https://doi.org/10.1149/05026.0375ecst.

[68] M.S. Ding, Q. Li, X. Li, W. Xu, K. Xu, Effects of solvent composition on liquid range, glass transition, and conductivity of electrolytes of a (Li, Cs)PF6 salt in EC-PC-EMC solvents, J. Phys. Chem. C 121 (2017) 11178–11183 https://doi.org/10.1021/acs.jpcc.7b03306.

[69] W.L. Jorgensen, D.S. Maxwell, J. Tirado-Rives, Development and testing of the OPLS all-atom force field on conformational energetics and properties of organic liquids, J. Am. Chem. Soc. 118 (1996) 11225–11236 https://doi.org/10.1021/ja9621760.

[70] G.A. Kaminski, R.A. Friesner, J. Tirado-Rives, W.L. Jorgensen, Evaluation and reparametrization of the OPLS-AA force field for proteins via comparison with accurate quantum chemical calculations on peptides†, J. Phys. Chem. B 105 (2001) 6474–6487 https://doi.org/10.1021/jp003919d.

[71] J.N.C. Lopes, A.A.H. Padua, Molecular force field for ionic liquids composed of triflate or bistriflylimide anions, J. Phys. Chem. B 108 (2004) 16893–16898 https://doi.org/10.1021/jp0476545.

[72] K.P. Jensen, W.L. Jorgensen, Halide, ammonium, and alkali metal ion parameters for modeling aqueous solutions, J. Chem. Theory Comput. 2 (2006) 1499–1509 https://doi.org/10.1021/ct600252r.

[73] A.D. Becke, Density-functional thermochemistry. III. The role of exact exchange, J. Chem. Phys. 98 (1993) 5648–5652 https://doi.org/10.1063/1.464913.

[74] M.J. Frisch, G.W. Trucks, H.B. Schlegel, G.E. Scuseria, M.A. Robb, J.R. Cheeseman, G. Scalmani, V. Barone, G.A. Petersson, H. Nakatsuji, X. Li, M. Caricato, A.V. Marenich, J. Bloino, B.G. Janesko, R. Gomperts, B. Mennucci, H.P. Hratchian, J.V. Ortiz, A.F. Izmaylov, J.L. Sonnenberg, Williams, F. Ding, F. Lipparini, F. Egidi, J. Goings, B. Peng, A. Petrone, T. Henderson, D. Ranasinghe, V.G. Zakrzewski, J. Gao, N. Rega, G. Zheng, W. Liang, M. Hada, M. Ehara, K. Toyota, R. Fukuda, J. Hasegawa, M. Ishida, T. Nakajima, Y. Honda, O. Kitao, H. Nakai, T. Vreven, K. Throssell, J.A. Montgomery Jr, J.E. Peralta, F. Ogliaro, M.J. Bearpark, J.J. Heyd, E. N. Brothers, K.N. Kudin, V.N. Staroverov, T.A. Keith, R. Kobayashi, J. Normand, K. Raghavachari, A.P. Rendell, J.C. Burant, S.S. Iyengar, J. Tomasi, M. Cossi, J.M. Millam, M. Klene, C. Adamo, R. Cammi, J.W. Ochterski, R.L. Martin, K. Morokuma, O. Farkas, J.B. Foresman, D.J. Fox, Wallingford, CT, 2016.

[75] C.I. Bayly, P. Cieplak, W.D. Cornell, P.A. Kollman, A well-behaved electrostatic potential based method using charge restraints for deriving atomic charges - the resp model, Chem. Phys. 97 (1993) 10269–10280 https://doi.org/10.1021/j100142a004.

[76] N.N. Rajput, V. Murugesan, Y. Shin, K.S. Han, K.C. Lau, J. Chen, J. Liu, L.A. Curtiss, K.T. Mueller, K.A. Persson, Elucidating the solvation structure and dynamics of lithium polysulfides resulting from competitive salt and solvent interactions, Chem. Mater. 29 (2017) 3375–3379 https://doi.org/10.1021/acs.chemmater.7b00068.

[77] A. Einstein, The motion of elements suspended in static liquids as claimed in the molecular kinetic theory of heat, Ann. Phys. Berl. 17 (1905) 549–560.

[78] D.M. Pesko, K. Timachova, R. Bhattacharya, M.C. Smith, I. Villaluenga, J. Newman, N.P. Balsara, Negative transference numbers in poly(ethylene oxide)-based electrolytes, J. Electrochem. Soc. 164 (2017) E3569–E3575 https://doi.org/10.1149/2.0581711jes.

[79] O. Borodin, M. Olguin, P. Ganesh, P.R. Kent, J.L. Allen, W.A. Henderson, Competitive lithium solvation of linear and cyclic carbonates from quantum chemistry, Phys. Chem. Chem. Phys. 18 (2016) 164–175 https://doi.org/10.1039/c5cp05121e.

[80] T.R. Jow, K. Xu, O. Borodin, M. Ue, Electrolytes for Lithium and Lithium-Ion Batteries, (2014).

[81] W. Ding, X. Lei, C. Ouyang, Coordination of lithium ion with ethylene carbonate electrolyte solvent: a computational study, Int. J. Quantum Chem. 116 (2016) 97–102 https://doi.org/10.1002/qua.25028.

[82] T.Z. Hou, W.T. Xu, X. Chen, H.J. Peng, J.Q. Huang, Q. Zhang, Lithium bond chemistry in lithium-sulfur batteries, Angew Chem. Int. Ed. Engl. 56 (2017) 8178–8182 https://doi.org/10.1002/anie.201704324.

[83] S. Grimme, J. Antony, S. Ehrlich, H. Krieg, A consistent and accurate ab initio parametrization of density functional dispersion correction (DFT-D) for the 94 elements H-Pu, J. Chem. Phys. 132 (2010) 154104 https://doi.org/10.1063/1.3382344.

[84] W. Cui, Y. Lansac, H. Lee, S.T. Hong, Y.H. Jang, Lithium ion solvation by ethylene carbonates in lithium-ion battery electrolytes, revisited by density functional theory with the hybrid solvation model and free energy correction in solution, Phys. Chem. Chem. Phys. 18 (2016) 23607–23612 https://doi.org/10.1039/c6cp01667g.

[85] K. Hagiyama, K. Suzuki, M. Ohtake, M. Shimada, N. Nanbu, M. Takehara, M. Ue, Y. Sasaki, Physical properties of substituted 1,3-Dioxolan-2-ones, Chem. Lett. 37 (2008) 210–211 https://doi.org/10.1246/cl.2008.210.

[86] B. Ravikumar, M. Mynam, B. Rai, Effect of salt concentration on properties of lithium ion battery electrolytes: a molecular dynamics study, J. Phys. Chem. C 122 (2018) 8173–8181 https://doi.org/10.1021/acs.jpcc.8b02072.

[87] T. Yoon, N. Chapman, D.M. Seo, B.L. Lucht, Lithium salt effects on silicon electrode performance and solid electrolyte interphase (SEI) structure, role of solution structure on SEI formation, J. Electrochem. Soc. 164 (2017) A2082–A2088 https://doi.org/10.1149/2.1421709jes.

[88] N. Chapman, O. Borodin, T. Yoon, C.C. Nguyen, B.L. Lucht, Spectroscopic and density functional theory characterization of common lithium salt solvates in carbonate electrolytes for lithium batteries, J. Phys. Chem. C 121 (2017) 2135–2148 https://doi.org/10.1021/acs.jpcc.6b12234.

[89] C.M. Tenney, R.T. Cygan, Analysis of molecular clusters in simulations of lithium-ion battery electrolytes, J. Phys. Chem. C 117 (2013) 24673–24684 https://doi.org/10.1021/jp4039122.

[90] K. Hayamizu, Temperature dependence of self-diffusion coefficients of ions and solvents in ethylene carbonate, propylene carbonate, and diethyl carbonate single solutions and ethylene carbonate + diethyl carbonate binary solutions of LiPF6 studied by NMR, J. Chem. Eng. Data 57 (2012) 2012–2017 https://doi.org/10.1021/je3003089.

[91] J. Wang, R.M. Wolf, J.W. Caldwell, P.A. Kollman, D.A. Case, Development and testing of a general amber force field, J. Comput. Chem. 25 (2004) 1157–1174 https://doi.org/10.1002/jcc.20035.

[92] S. Burlatsky, R.M. Darling, D. Novikov, V.V. Atrazhev, V.I. Sultanov, T.Y. Astakhova, L. Su, F. Brushett, Molecular dynamics modeling of the conductivity of lithiated nafion containing nonaqueous solvents, J. Electrochem. Soc. 163 (2016) A2232–A2239 https://doi.org/10.1149/2.0461610jes.

[93] X. Chen, T. Hou, K.A. Persson, Q. Zhang, Combining theory and experiment in lithium–sulfur batteries: current progress and future perspectives, Mater. Today 22 (2019) 142–158 https://doi.org/10.1016/j.mattod.2018.04.007.

[94] B. Fortunato, P. Mirone, G. Fini, Infrared and Raman spectra and vibrational assignment of ethylene carbonate, Spectrochim. Acta Mol. Spectros 27 (1971) 1917–1927 https://doi.org/10.1016/0584-8539(71)80245-3.

[95] J.L. Allen, O. Borodin, D.M. Seo, W.A. Henderson, Combined quantum chemical/Raman spectroscopic analyses of Li+ cation solvation: cyclic carbonate solvents—ethylene carbonate and propylene carbonate, J. Power Sources 267 (2014) 821–830 https://doi.org/10.1016/j.jpowsour.2014.05.107.

[96] Y. Horowitz, H.L. Han, F.A. Soto, W.T. Ralston, P.B. Balbuena, G.A. Somorjai, Fluoroethylene carbonate as a directing agent in amorphous silicon anodes: electrolyte interface structure probed by sum frequency vibrational spectroscopy and ab initio molecular dynamics, Nano Lett. 18 (2018) 1145–1151 https://doi.org/10.1021/acs.nanolett.7b04688.

[97] Y. Horowitz, H.G. Steinruck, H.L. Han, C. Cao, Abate II, Y. Tsao, M.F. Toney, G.A. Somorjai, Fluoroethylene carbonate induces ordered electrolyte interface on silicon and sapphire surfaces as revealed by sum frequency generation vibrational spectroscopy and X-ray reflectivity, Nano Lett. 18 (2018) 2105–2111 https://doi.org/10.1021/acs.nanolett.8b00298.

[98] J.C. Soetens, C. Millot, B. Maigret, Molecular dynamics simulation of Li(+)BF4(-)

[99] in ethylene carbonate, propylene carbonate, and dimethyl carbonate solvents, J. Phys. Chem. A 102 (1998) 1055–1061 https://doi.org/10.1021/jp972457+.

[99] I. Skarmoutsos, V. Ponnuchamy, V. Vetere, S. Mossa, Li+ solvation in pure, binary, and ternary mixtures of organic carbonate electrolytes, J. Phys. Chem. C 119 (2015) 4502–4515 https://doi.org/10.1021/jp511132c.

[100] C. Liang, K. Kwak, M. Cho, Revealing the solvation structure and dynamics of carbonate electrolytes in lithium-ion batteries by two-dimensional infrared spectrum modeling, J. Phys. Chem. Lett. 8 (2017) 5779–5784 https://doi.org/10.1021/acs.jpclett.7b02623.

[101] D.M. Seo, S. Reininger, M. Kutcher, K. Redmond, W.B. Euler, B.L. Lucht, Role of mixed solvation and ion pairing in the solution structure of lithium ion battery electrolytes, J. Phys. Chem. C 119 (2015) 14038–14046 https://doi.org/10.1021/acs.jpcc.5b03694.

[102] X. Bogle, R. Vazquez, S. Greenbaum, A. Cresce, K. Xu, Understanding Li(+)-Solvent interaction in nonaqueous carbonate electrolytes with (17)O NMR, J. Phys. Chem. Lett. 4 (2013) 1664–1668 https://doi.org/10.1021/jz400661k.

[103] P. Ganesh, D.E. Jiang, P.R. Kent, Accurate static and dynamic properties of liquid electrolytes for Li-ion batteries from ab initio molecular dynamics, J. Phys. Chem. B 115 (2011) 3085–3090 https://doi.org/10.1021/jp2003529.

[104] M.I. Chaudhari, J.R. Nair, L.R. Pratt, F.A. Soto, P.B. Balbuena, S.B. Rempe, Scaling atomic partial charges of carbonate solvents for lithium ion solvation and diffusion, J. Chem. Theory Comput. 12 (2016) 5709–5718 https://doi.org/10.1021/acs.jctc.6b00824.

[105] R. Jorn, R. Kumar, D.P. Abraham, G.A. Voth, Atomistic modeling of the electrode–electrolyte interface in Li-ion energy storage systems: electrolyte structuring, J. Phys. Chem. C 117 (2013) 3747–3761 https://doi.org/10.1021/jp3102282.

[106] O. Borodin, G.D. Smith, Quantum chemistry and molecular dynamics simulation study of dimethyl carbonate: ethylene carbonate electrolytes doped with LiPF6, J. Phys. Chem. B 113 (2009) 1763–1776 https://doi.org/10.1021/jp809614h.

[107] K.K. Lee, K. Park, H. Lee, Y. Noh, D. Kossowska, K. Kwak, M. Cho, Ultrafast fluxional exchange dynamics in electrolyte solvation sheath of lithium ion battery, Nat. Commun. 8 (2017) 14658 https://doi.org/10.1038/ncomms14658.

[108] J. Xia, R. Petibon, A. Xiao, W.M. Lamanna, J.R. Dahn, Some fluorinated carbonates as electrolyte additives for Li(Ni0.4Mn0.4Co0.2)O2/graphite pouch cells, J. Electrochem. Soc. 163 (2016) A1637–A1645 https://doi.org/10.1149/2.0831608jes.

[109] A. von Wald Cresce, O. Borodin, K. Xu, Correlating Li+ solvation sheath structure with interphasial chemistry on graphite, J. Phys. Chem. C 116 (2012) 26111–26117 https://doi.org/10.1021/jp303610t.

[110] J. Xia, R. Petibon, D. Xiong, L. Ma, J.R. Dahn, Enabling linear alkyl carbonate electrolytes for high voltage Li-ion cells, J. Power Sources 328 (2016) 124–135 https://doi.org/10.1016/j.jpowsour.2016.08.015.

[111] K. Leung, Predicting the voltage dependence of interfacial electrochemical processes at lithium-intercalated graphite edge planes, Phys. Chem. Chem. Phys. 17 (2015) 1637–1643 https://doi.org/10.1039/c4cp04494k.

[112] V. Etacheri, O. Haik, Y. Goffer, G.A. Roberts, I.C. Stefan, R. Fasching, D. Aurbach, Effect of fluoroethylene carbonate (FEC) on the performance and surface chemistry of Si-nanowire Li-ion battery anodes, Langmuir 28 (2012) 965–976 https://doi.org/10.1021/la203712s.

[113] E. Markevich, K. Fridman, R. Sharabi, R. Elazari, G. Salitra, H.E. Gottlieb, G. Gershinsky, A. Garsuch, G. Semrau, M.A. Schmidt, D. Aurbach, Amorphous columnar silicon anodes for advanced high voltage lithium ion full cells: dominant factors governing cycling performance, J. Electrochem. Soc. 160 (2013) A1824–A1833 https://doi.org/10.1149/2.085310jes.

[114] K. Kim, I. Park, S.-Y. Ha, Y. Kim, M.-H. Woo, M.-H. Jeong, W.C. Shin, M. Ue, S.Y. Hong, N.-S. Choi, Understanding the thermal instability of fluoroethylene carbonate in LiPF 6 -based electrolytes for lithium ion batteries, Electrochim. Acta 225 (2017) 358–368 https://doi.org/10.1016/j.electacta.2016.12.126.

[115] K. Sodeyama, Y. Yamada, K. Aikawa, A. Yamada, Y. Tateyama, Sacrificial anion reduction mechanism for electrochemical stability improvement in highly concentrated Li-salt electrolyte, J. Phys. Chem. C 118 (2014) 14091–14097 https://doi.org/10.1021/jp501178n.

[116] J. Qian, W.A. Henderson, W. Xu, P. Bhattacharya, M. Engelhard, O. Borodin, J.G. Zhang, High rate and stable cycling of lithium metal anode, Nat. Commun. 6 (2015) 6362 https://doi.org/10.1038/ncomms7362.

[117] Y.B. Yohannes, S.D. Lin, N.-L. Wu, In situ DRIFTS analysis of solid electrolyte interphase of Si-based anode with and without fluoroethylene carbonate additive, J. Electrochem. Soc. 164 (2017) A3641–A3648 https://doi.org/10.1149/2.0681714jes.

[118] Y. Horowitz, H.L. Han, W.T. Ralston, J.R. de Araujo, E. Kreidler, C. Brooks, G.A. Somorjai, Fluorinated end-groups in electrolytes induce ordered electrolyte/anode interface even at open-circuit potential as revealed by sum frequency generation vibrational spectroscopy, Adv. Energy Mater. 7 (2017) 1602060 https://doi.org/10.1002/aenm.201602060.

[119] J. Nanda, G. Yang, T. Hou, D.N. Voylov, X. Li, R.E. Ruther, M. Naguib, K. Persson, G.M. Veith, A.P. Sokolov, Unraveling the Nanoscale Heterogeneity of Solid Electrolyte Interphase Using Tip-Enhanced Raman Spectroscopy, Joule (2019), https://doi.org/10.1016/j.joule.2019.05.026.
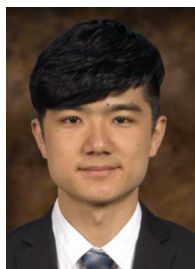
Tingzheng Hou is a Ph.D. student in Materials Science and Engineering at the University of California, Berkeley, supervised by Prof. Kristin Persson. He earned his bachelor's degree in materials science and Engineering, and a master's degree in chemical engineering both from Tsinghua University, China, in 2014 and 2016. He previously worked on computational modeling and rational design of lithium–sulfur batteries and lithium metal batteries in Qiang Zhang's group in Tsinghua. He is now focusing on the modeling and simulation of novel electrolyte systems for silicon anode materials.

Sang-Won Park received his Ph.D. in Chemistry in 2016 from Seoul National University in Seoul, Korea. He joined UC Berkeley as a postdoctoral fellow at the Department of Materials Science and Engineering in 2017. His research is focused on energy devices of soft materials which are based on simulations and theories of statistical mechanics. He is currently working as a postdoc in Molecular Foundry of Lawrence Berkeley National Laboratory.
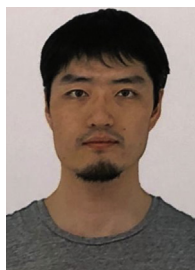
Guang Yang is a Postdoc Research Associate at Oak Ridge National Laboratory (ORNL) mentored by Dr. Jagjit Nanda. He obtained his bachelor's degree in biomedical engineering from Southeast University, China in 2009, and a master degree in Advanced Materials program from University of Ulm, Germany, 2012. He is a chemical engineer with a Ph.D. degree from Florida State University (supervised by Dr. Daniel Hallinan). His research is focused on exploring the electrolyte structure at the solid/liquid electrolyte interface, the solution structure of solid polymer electrolyte, and the structure and evolution of the solid-electrolyte interphase (SEI) using plasmon-enhanced Raman spectroscopy.

Jagjit Nanda is currently a Team Lead and Senior Staff scientist at Oak Ridge National Laboratory (ORNL)'s Chemical Sciences Division, working in the area of high capacity energy storage materials, interfaces and energy systems. He is a joint professor in Chemical and Biomolecular Engineering Dept., University of Tennessee, Knoxville. Prior to joining ORNL, Jagjit worked as a Technical Expert at the Research and Advanced Engineering Center, Ford Motor Company, leading R&D projects in lithium-ion battery materials. He has > 150 journal publications, 50 invited talks and several patents on energy storage and conversion and holds membership of many professional scientific societies.

Nav Nidhi Rajput is an assistant professor in the Department of Chemical and Biological Engineering at Tufts University. She received her M.S. and Ph.D. degrees in Chemical Engineering at the Louisiana State University. Before joining Tufts University in 2018 Dr. Rajput carried out postdoctoral research at Lawrence Berkeley National Laboratory, where she was working on the designing optimal electrolytes for battery technologies. Her scientific interests are focused on predicting and understanding the unique chemical and physical properties of liquid solutions, nanoporous materials, and confined fluids—using computer simulations—for applications in nanostructured materials and energy storage.

Kristin Aslaug Persson obtained her Ph.D. in Theoretical Physics at the Royal Institute of Technology in Stockholm, Sweden in 2001. She is a Professor in Materials Science and Engineering at UC Berkeley with a joint appointment as Faculty Staff Scientist at LBNL. Persson is the Director and co-founder of the Materials Project (www.materialsproject.org) and known for her advancement of data-driven materials design and materials informatics. Interests include materials in extreme pH environments, novel multivalent electrode and electrolyte materials, novel photocatalysts for water splitting and CO_2 reduction, and new polar materials. She has over 150 publications, and several patents in the broad area of materials for clean energy applications.
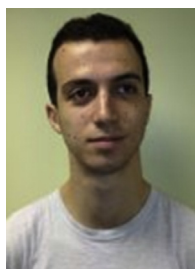
Julian Self is a Ph.D. candidate in Materials Science and Engineering at the University of California, Berkeley, working in Kristin Persson's group. He previously received a M. Sc. from Dalhousie University under the supervision of Jeff Dahn. His interests include Li-ion and multivalent ion batteries, and more generally the electrochemistry and physical chemistry of liquid electrolytes for energy storage applications.